Transport properties and equation-of-state of hot and dense QGP matter near the critical endpoint in the phenomenological dynamical quasiparticle model

Olga Soloveva,[1,2,*] Jörg Aichelin,[3,4] and Elena Bratkovskaya[5,2,1]

[1]*Helmholtz Research Academy Hesse for FAIR (HFHF), GSI Helmholtz Center for Heavy Ion Physics, Campus Frankfurt, 60438 Frankfurt, Germany*

[2]*Institut für Theoretische Physik, Johann Wolfgang Goethe-Universität, Max-von-Laue-Straße 1, D-60438 Frankfurt am Main, Germany*

[3]*SUBATECH, University of Nantes, IMT Atlantique, IN2P3/CNRS 4 rue Alfred Kastler, 44307 Nantes cedex 3, France*

[4]*Frankfurt Institute for Advanced Studies, Ruth Moufang Straße. 1, 60438 Frankfurt, Germany*

[5]*GSI Helmholtzzentrum für Schwerionenforschung GmbH, Planckstrasse 1, D-64291 Darmstadt, Germany*

(Received 23 August 2021; accepted 28 January 2022; published 14 March 2022)

We extend the effective dynamical quasiparticle model (DQPM)—constructed for the description of nonperturbative QCD phenomena of the strongly interacting quark-gluon plasma (QGP)—to large baryon chemical potentials, μ_B, including a critical endpoint (CEP) and a first-order phase transition. The DQPM description of quarks and gluons is based on partonic propagators with complex self-energies where the real part of the self-energies is related to the quasiparticle mass and the imaginary part to a finite width of their spectral functions (i.e., the imaginary parts of the propagators). In DQPM the determination of complex self-energies for the partonic degrees of freedom at zero and finite μ_B has been performed by adjusting the entropy density to the lattice QCD data. The temperature-dependent effective coupling (squared) $g^2(T/T_c)$, as well as the effective masses and widths of the partons are based on this adjustments. The novel extended dynamical quasiparticle model, named "DQPM-CP," makes it possible to describe thermodynamical and transport properties of quarks and gluons in a wide range of temperature, T, and baryon chemical potential, μ_B, and reproduces the equation of state of lattice QCD calculations in the crossover region of finite T, μ_B. We apply a scaling ansatz for the strong coupling constant near the CEP, located at $(T^{\mathrm{CEP}}, \mu_B^{\mathrm{CEP}}) = (0.100, 0.960)$ GeV. We show the equation of state as well as the speed of sound for $T > T_c$ and for a wide range of μ_B, which can be of interest for hydrodynamical simulations. Furthermore, we consider two settings for the strange quark chemical potentials, (I) $\mu_q = \mu_u = \mu_s = \mu_B/3$ and (II) $\mu_s = 0, \mu_u = \mu_d = \mu_B/3$. The isentropic trajectories of the quark-gluon plasma matter are compared for these two cases. The phase diagram of DQPM-CP is close to PNJL calculations. The leading order pQCD transport coefficients of both approaches differ. This elucidates that the knowledge of the phase diagram alone is not sufficient to describe the dynamical evolution of strongly interacting matter.

DOI: 10.1103/PhysRevD.105.054011

I. INTRODUCTION

The extension of the QCD phase diagram to a finite baryon chemical potential is a challenging task. It is believed that QCD matter undergoes a phase transition from the confined hadronic phase to the deconfined QGP phase if one increases the chemical potential at moderate temperatures and the transition line in (T, μ_B) is expected to terminate at a critical endpoint. This is the least explored area of the QCD phase diagram but of particular interest for future experimental programs and theoretical studies (see the recent review [1]). To realize these studies in a viscous hydrodynamical model, one has to know the equation of state (EoS) of strongly interacting matter but also the transport coefficients. The time evolution of the QGP medium, produced in heavy-ion collisions (HICs), can also be addressed in microscopic transport approaches, which provide the time evolution of the degrees of freedom of the system. They require, in addition, the knowledge of

*soloveva@itp.uni-frankfurt.de

the microscopic properties of the partonic degrees of freedom, such as effective masses, widths, and cross sections, which all may depend on μ_B and T. The large value of the running coupling requires nonperturbative methods, such as lattice QCD (lQCD) calculations, or effective models with a phenomenological input. Therefore, it is notoriously difficult to estimate thermodynamic properties of the deconfined QCD matter, especially in the vicinity of a phase transition.

The lQCD calculations at vanishing baryon chemical potential are well established. However, due to the fermion sign problem, it is not at all easy to extend these calculations to a large baryon chemical potential. One possibility for exploring thermodynamic functions at $\mu_B > 0$ is to employ a Taylor expansion of the partition function in the vicinity of $\mu_B = 0$. It shares with other approaches, which were designed for $\mu_B = 0$, that the uncertainty of the predictions increases with the increase of μ_B.

Here we present a new phenomenological model, the generalized quasiparticle model, DQPM-CP, for the description of nonperturbative features of the (strongly interacting) QCD. It reproduces the lQCD EoS for $\mu_B = 0$ as well as the first coefficient of the Taylor expansion towards finite μ_B but can be extended to a wide range of μ_B. For this we combine the findings of DQPM, with a new parametrization of the coupling constant. One of the important features of the DQPM-CP is the appearance of "critical" scaling in the vicinity of the critical endpoint (CEP). The main goal of the DQPM-CP is to provide the microscopic and macroscopic properties of the partonic degrees of freedom for the region of the phase diagram which is characterized by moderate T and moderate or high μ_B. Their knowledge allows us subsequently to calculate the transport coefficients as well as the EoS, the ingredients of viscous hydrodynamic calculations.

In the present study we employ results from different methods such as lQCD calculations and results from the $N_f = 3$ PNJL model extended beyond the mean field, because more rigorous approaches, such as Dyson-Schwinger equations [2], functional renormalization group [3], or pQCD/HTL calculations [4] can currently not cover the interesting observables in the full (T, μ_B) plane. There are no fully consistent calculations within a single approach, which includes the QGP thermodynamic observables and simultaneously the transport coefficients for the region of moderate and high μ_B or μ_q. The presented results are model dependent, however, qualitatively in agreement with the results from various effective models such as PNJL, NJL, LSM, and nonconformal holographic models. Only at moderate baryon density can we compare the more rigorous methods such as lQCD, functional renormalization group, nad Dyson-Schwinger equations. Nevertheless, the demand for an EoS and transport coefficients at moderate and high baryon chemical potentials is high due to the ongoing investigation of HICs by transport or/and hydrodynamic models [1]. These investigations aim at the exploration of observables, which may carry information about this region of the phase diagrams. Therefore the presented results, even if they allow only for qualitative predictions, can be useful for transport studies, which have multiple issues to solve in the region of moderate baryon density while awaiting results from more rigorous approaches.

The main advantage of the use of quasiparticle models is the simple implementation in the transport framework for the evolution of the QGP matter. The DQPM has been implemented in the PHSD transport approach [5,6], whereas the QPM [7] is implemented in the Catania transport approach [8]. Recently also, results from approximate models of QCD, like that from NJL and PNJL models, have been implemented in the AMPT model [9] via scalar and vector potentials. The goal of the presented model is to interpolate the EoS and partonic properties such as effective masses, scalar potential, and cross sections between the region of high T and $\mu_B = 0$ to the region of moderate T and high μ_B. In particular, we are currently working on the implementation of the DQPM-CP in the PHSD transport approach [5,6].

The degrees of freedom of the DQPM are strongly interacting dynamical quasiparticles—quarks and gluons—with a broad spectral function, whose "thermal" masses and widths increase with growing temperature. The knowledge of the T and μ_B dependence of the mass of our degrees of freedom allows for the calculation of transport coefficients in lowest order in pQCD. They can be compared with the transport coefficients, calculated recently in the PNJL approach, which has a very similar phase diagram but other degrees of freedom (interacting massless quarks and no gluons). The comparison of the transport coefficients shows that they depend indeed on the properties of the degrees of freedom and may be rather different in two theories with almost the same phase diagram.

The paper is organized as follows: In Sec. II we give a brief review of the basic ingredients of the dynamical quasiparticle model and its extension to the finite μ_B region. In Sec. III we discuss the thermodynamic observables for two setups of quark chemical potential: (I) $\mu_q = \mu_u = \mu_s = \mu_B/3$ and (II) $\mu_s = 0, \mu_u = \mu_d = \mu_B/3$. Furthermore, we study second-order derivatives of the partition function, such as speed of sound and specific heat and isentropic trajectories of the QGP matter. Further, in Sec. IV we present transport coefficients of the DQPM-CP such as the specific shear viscosity and ratio of electric σ_{QQ}/T, baryon σ_{BB}/T, and strange σ_{SS}/T conductivities to temperature based on the relaxation time approximation of the Boltzmann equation. In addition, we show the ratio of dimensionless transport coefficients for the full range of chemical potentials. We finalize our study with conclusions in Sec. V.

II. BASIC PROPERTIES OF THE QUASIPARTICLE MODEL

A. Main ingredients of the off-shell quasiparticle models

In the dynamical quasiparticle model, DQPM [6,10–12], the QGP medium is described in terms of strongly interacting quasiparticles, quarks and gluons. The quasiparticles are massive and can be characterized by broad spectral functions ρ_i $(i = q, \bar{q}, g)$, which are no longer δ functions in the invariant mass squared but are given by

$$\rho_i(\omega, \mathbf{p}) = \frac{\gamma_i}{\tilde{E}_{i,\mathbf{p}}}\left(\frac{1}{(\omega - \tilde{E}_{i,\mathbf{p}})^2 + \gamma_i^2} - \frac{1}{(\omega + \tilde{E}_{i,\mathbf{p}})^2 + \gamma_i^2}\right) = \frac{4\omega\gamma_i}{(\omega^2 - \mathbf{p}^2 - m_i^2)^2 + 4\gamma_i^2\omega^2}. \quad (1)$$

Here, we introduced the off-shell energy $\tilde{E}_{i,\mathbf{p}} = \sqrt{\mathbf{p}^2 + m_i^2 - \gamma_i^2}$, with m_i,γ_i being the pole mass and width, which differ for quarks, antiquarks, and gluons. Then the quasiparticle (retarded) propagators can be expressed in the Lehmann representation via the spectral function:

$$\Delta_i(\omega, \mathbf{p}) = \int_{-\infty}^{\infty} \frac{d\omega'}{2\pi}\frac{\rho_i(\omega', \mathbf{p})}{\omega - \omega'} = \frac{1}{\omega^2 - \mathbf{p}^2 - m_i^2 + 2i\gamma_i\omega}. \quad (2)$$

The quasiparticle pole masses for gluons and quarks are defined, inspired by the asymptotic HTL masses [13,14], by

$$m_g^2(T, \mu_\mathrm{B}) = C_g\frac{g^2(T, \mu_\mathrm{B})}{6}T^2\left(1 + \frac{N_f}{2N_c} + \frac{1}{2}\frac{\sum_q \mu_q^2}{T^2\pi^2}\right) \quad (3)$$

$$m_{q(\bar{q})}^2(T, \mu_\mathrm{B}) = C_q\frac{g^2(T, \mu_\mathrm{B})}{4}T^2\left(1 + \frac{\mu_q^2}{T^2\pi^2}\right), \quad (4)$$

where $N_c = 3$ and $N_f = 3$ denote the number of colors and the number of flavors, respectively. $C_q = \frac{N_c^2 - 1}{2N_c} = 4/3$ and $C_g = N_c = 3$ are the QCD color factors for quarks and for gluons, respectively. The strange quark has a larger bare mass which needs to be considered in its dynamical quasiparticle pole mass. We fix $m_s(T, \mu_\mathrm{B}) = m_u(T, \mu_\mathrm{B}) + \Delta m$ and $\Delta m \approx 30$ MeV [6].

Furthermore, the quasiparticles in DQPM have thermal widths, which are adopted in the form [14,15]

$$\gamma_j(T, \mu_\mathrm{B}) = \frac{1}{3}C_j\frac{g^2(T, \mu_\mathrm{B})T}{8\pi}\ln\left(\frac{2c_m}{g^2(T, \mu_\mathrm{B})} + 1\right). \quad (5)$$

The parameter c_m, which is related to a magnetic cutoff, is fixed to $c_m = 14.4$.

In the DQPM, the coupling constant at $\mu_B = 0$ is parametrized, employing the entropy density $s(T, \mu_\mathrm{B} = 0)$ from lattice QCD calculations of Refs. [16,17] in the following way:

$$g^2(T, \mu_\mathrm{B} = 0) = d((s(T, 0)/s_\mathrm{SB}^\mathrm{QCD})^e - 1)^f, \quad (6)$$

with the Stefan-Boltzmann entropy density $s_\mathrm{SB}^\mathrm{QCD}/T^3 = 19/9\pi^2$ and the dimensionless parameters $d = 169.934$, $e = -0.178434$, and $f = 1.14631$.

We note that the DQPM has been used to explore the crossover region in the phase diagram by introducing an effective coupling constant which depends on the baryon chemical potential. In this region of a moderate baryon chemical potential, the basic thermodynamic observables, computed in lQCD, show a smooth μ_B dependence. Therefore we expect a similar behavior for the effective coupling.

The effective coupling at finite baryon chemical potential μ_B is obtained by applying the "'scaling hypothesis" introduced in [11]. It assumes that g^2 is a function of the ratio of the effective temperature

$$T^* = \sqrt{T^2 + \mu_q^2/\pi^2} \quad (7)$$

(where the quark chemical potential is defined as $\mu_q = \mu_u = \mu_s = \mu_B/3$) and the μ_B-dependent critical temperature $T_c(\mu_\mathrm{B})$ as [15]

$$T_c(\mu_B) = T_c(0)(1 - \alpha\mu_B^2)^{1/2}, \quad (8)$$

where $T_c(0)$ is the critical temperature at vanishing chemical potential ($\approx$0.158 GeV) and $\alpha = 0.974$ GeV^{-2}. Thus, the DQPM effective coupling $\alpha_S^\mathrm{DQPM}(T, \mu_\mathrm{B})$ reads

$$\alpha_S^\mathrm{DQPM}(T, \mu_\mathrm{B}) \equiv \begin{cases} \mu_\mathrm{B} = 0: & g^2(T, \mu_\mathrm{B} = 0)/(4\pi) \\ \mu_\mathrm{B} > 0: & g^2(T_\mathrm{scale}(T, \mu_\mathrm{B}))/(4\pi), \\ \text{With} & T_\mathrm{scale} = \frac{T^*}{T_c(\mu_\mathrm{B})/T_c(0)}. \end{cases} \quad (9)$$

Having fixed the quasiparticle properties (or propagators) as described above, one can evaluate the basic thermodynamic observables: the entropy density $s(T, \mu_B)$, the pressure $P(T, \mu_B)$, and energy density $\epsilon(T, \mu_B)$ in a straight forward manner by starting with the quasiparticle entropy density and number density. The entropy density and the quark number density follow from the same thermodynamic potential $\Omega[\Delta, S_q]$ [18,19], which is expressed as a functional of the full quasiparticle propagators for gluons and quarks(Δ, S_q) in a symmetry-conserving ("Φ derivable") two-loop approximation:

$$
\begin{aligned}
&s^{dqp} \\
&= -d_g \int \frac{d\omega}{2\pi}\frac{d^3p}{(2\pi)^3}\frac{\partial f_g}{\partial T}(\mathrm{Im}(\ln\Delta^{-1}) - \mathrm{Im}\Pi \times \mathrm{Re}\Delta) \\
&\quad - d_q \int \frac{d\omega}{2\pi}\frac{d^3p}{(2\pi)^3}\frac{\partial f_q(\omega-\mu_q)}{\partial T}(\mathrm{Im}(\ln S_q^{-1}) - \mathrm{Im}\Sigma_q \mathrm{Re}S_q) \\
&\quad - d_{\bar{q}} \int \frac{d\omega}{2\pi}\frac{d^3p}{(2\pi)^3}\frac{\partial f_{\bar{q}}(\omega+\mu_q)}{\partial T}(\mathrm{Im}(\ln S_{\bar{q}}^{-1}) - \mathrm{Im}\Sigma_{\bar{q}} \mathrm{Re}S_{\bar{q}})
\end{aligned} \tag{10}
$$

$$
\begin{aligned}
&n^{dqp} \\
&= -d_q \int \frac{d\omega}{2\pi}\frac{d^3p}{(2\pi)^3}\frac{\partial f_q(\omega-\mu_q)}{\partial \mu_q}(\mathrm{Im}(\ln S_q^{-1}) - \mathrm{Im}\Sigma_q \mathrm{Re}S_q) \\
&\quad - d_{\bar{q}} \int \frac{d\omega}{2\pi}\frac{d^3p}{(2\pi)^3}\frac{\partial f_{\bar{q}}(\omega+\mu_q)}{\partial \mu_q}(\mathrm{Im}(\ln S_{\bar{q}}^{-1}) - \mathrm{Im}\Sigma_{\bar{q}} \mathrm{Re}S_{\bar{q}})
\end{aligned} \tag{11}
$$

where $f_g(\omega)$ and $f_q(\omega-\mu_q)$ denote the Bose-Einstein and Fermi-Dirac distribution functions [see Eq. (25)], respectively, while $\Delta = (p^2-\Pi)^{-1}$, $S_q = (p^2-\Sigma_q)^{-1}$, and $S_{\bar{q}} = (p^2-\Sigma_{\bar{q}})^{-1}$ stand for the full (scalar) quasiparticle propagator of gluons g, quarks q, and antiquarks $\bar{q}$. In Eqs. (10) and (11) we consider for simplicity, scalar (retarded) quasiparticle self-energies $\Pi = \Sigma = \Sigma_q \approx \Sigma_{\bar{q}}$, which are expressed via dynamical masses and widths as $\Pi = m_i^2 - 2i\gamma_i\omega_i$, where, for the off-shell case, ω_i is an independent variable. Furthermore, the number of transverse gluonic degrees of freedom is $d_g = 2\times(N_c^2-1)$ while for the fermion degrees of freedom we use $d_q = 2\times N_c$ and $d_{\bar{q}} = 2\times N_c$.

B. Extension of quasiparticle DQPM-CP effective coupling constant for the inclusion of the CEP

Now we proceed with the extension of the DQPM to the region of large μ_B where a possible critical endpoint is located. In order to extend the quasiparticle model to the large μ_B region and to describe the critical behavior near the CEP we depart from the "scaling hypothesis" used for the moderate baryon chemical potentials in the crossover region and introduce a simple parametrization of the coupling constant as a function of the scaled temperature and the baryon chemical potential. To simplify an extension of the effective coupling for finite μ_B we parametrize $\alpha_s^{\mathrm{DQPM-CP}}$ as a function of a dimensionless scaled temperature $x_T = T/T_c$. We determine first the parameters at vanishing quark or baryon chemical potential by fitting extracted values of $g^2_{\mathrm{DQPM}}(T,\mu_B=0)$ from Eq. (6) as a function $f(T/T_c,\mu_B=0)$ ($T_c = 0.158$) with the help of the nonlinear least-squares Marquardt-Levenberg algorithm. Later we use critical line values of T_c for each value of the baryon chemical potential. The critical line of the present model, which is an input parameter for our calculations, reads

$$
T_c(\mu_B) = T_c(0)[1-\kappa_{\mathrm{PNJL}}(\mu_B/T_c(0))^2], \tag{12}
$$

where $T_c(0) = 0.158$ GeV is fixed in accordance with the results from lQCD [20,21], while $\kappa_{\mathrm{PNJL}} = 0.00989$ corresponds to the estimates from the PNJL model [22].

Figure 1 shows a comparison of the critical lines of the DQPM (green dashed line), of the DQPM-CP, and the predictions from the lQCD calculations. The DQPM-CP phase boundary, given by Eq. (12), is shown as a black dashed-dotted line in the crossover region, i.e., for moderate baryon chemical potentials. The critical endpoint in the presented model is located at $(T^{\mathrm{CEP}},\mu_B^{\mathrm{CEP}}) = (0.100, 0.960)$ GeV.

The exact location of the CEP is an open question and there are many predictions from various methods [for a compilation of theoretical predictions for $(T^{\mathrm{CEP}},\mu_B^{\mathrm{CEP}})$ we refer the reader to Fig. 6 in Ref. [24], and to Fig. 19 in Ref. [25]]. Current state-of-the-art lQCD results disfavor a critical point for $\mu_B/T \lesssim 3$ [16,21,26,27]. Furthermore, it has been found that the temperature of the hypothetical chiral critical endpoint should not exceed the critical temperature of the chiral phase transition (for $m_u = m_d = 0$) $T_c^0 = 132^{+3}_{-6}$ MeV [28,29]. Recently, the approximate position of the chiral CEP (for vanishing external magnetic field) of $\mu_B^{\mathrm{CEP}} = 0.800(0.140)$ GeV has been conjectured by the lQCD simulations of finite density QGP under external

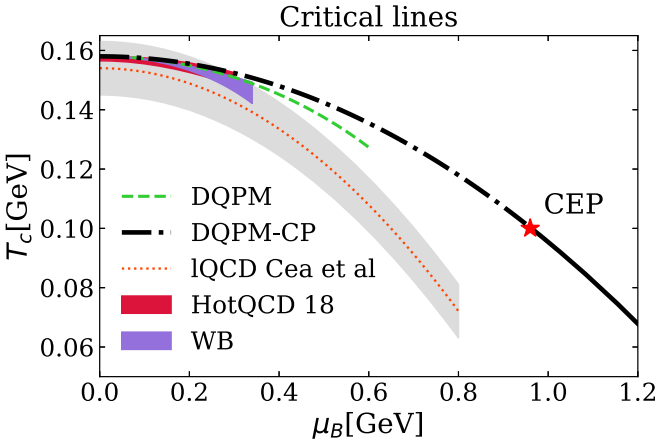

FIG. 1. Critical line of the DQPM-CP (black lines) and of the DQPM (green dashed line) in the (T,μ_B) plane of the QCD phase diagram. DQPM-CP ($\mu_q = \mu_s = \mu_B/3$): The finite temperature crossover (black dash-dotted line) at small chemical potential switches to a first-order transition (black solid line) at the hypothetical CEP (red star), which is located at (0.10,0.96) GeV. DQPM ($\mu_q = \mu_s = \mu_B/3$): The finite temperature crossover (green dashed line). Lines with colored areas represent lQCD estimates of $T_c(\mu_B)$ for QCD with $N_f = 2+1$: ($\mu_q = \mu_s = \mu_B/3$) grey area, from Ref. [23]; ($\mu_q = \mu_s = \mu_B/3$) red area, from Ref. [20]; ($\langle n_S\rangle = 0$) violet area, from Ref. [21].

magnetic fields [30]. It has been shown that the critical line of the PNJL model generally depends on the parameters of the model [31]. Many (P)NJL model predictions of the location of the CEP lie at high $\mu_B \sim 0.8-1$ GeV [24]; for instance, for the $N_f = 2$ NJL model in Ref. [32] $(T^{\mathrm{CEP}}, \mu_B^{\mathrm{CEP}}) = (0.081, 0.987)$ GeV $(\mu_B^{\mathrm{CEP}} = 3\mu_q^{\mathrm{CEP}})$, while for the $N_f = 3$ PNJL model considered in Ref. [33] $(T^{\mathrm{CEP}}, \mu_B^{\mathrm{CEP}}) = (0.121, 0.875)$ GeV.

We base this study on the predictions from the extended beyond mean field $N_f = 3$ PNJL model [22]. However, in order to fit lattice results at moderate $\mu_B \leq 0.6$ GeV we use the value of the pseudocritical temperature at $\mu_B = 0$ from lQCD estimates. First, the value of the baryon chemical potential of the hypothetical CEP μ_B^{CEP} is chosen in accord with predictions from the PNJL model, then the temperature of the CEP follows from the chosen critical line $T_c(\mu_B)$. The chosen location of the hypothetical CEP is within the allowed range of the lQCD estimates. The first-order phase transition is shown as a solid black line. The DQPM phase boundary for moderate baryon chemical potentials, $\mu_B \leq 0.6$ GeV, given by Eq. (8), is shown as a dashed green line. The colored areas illustrate the predictions from the lQCD calculations for QCD with $N_f = 2+1$: grey area, from Ref. [23]; red area, from Ref. [20]; violet area, from Ref. [21].

To interpolate the EoS and microscopic properties of quarks and gluons between the region of the vanishing baryon chemical potential and the asymptotic behavior in the region of high baryon density $\mu_B \gg T$ $(T > T_c(\mu_B))$, we employ a simple ansatz for the μ_B dependence, which reflects the decrease of the effective coupling with μ_B. We assume that the coupling constant does not depend explicitly on the temperature but only on the scaled temperature $[x_T = T/T_c(\mu_B)]$ (T_c varies with μ_B according to the chosen critical line) for all $\mu_B \geq 0$. Furthermore, we introduce an additional factor $\sigma(\mu_B)(= 1 \text{ at } \mu_B = 0)$ to take into account the decrease of the coupling constant with μ_B at moderate x_T. At high T $(T/T_c(\mu_B) \equiv x_T \gg 1)$ the effective coupling constant is not affected by the baryon chemical potential. Therefore, the DQPM-CP coupling constant can be parametrized as a function of a scaled temperature and μ_B:

$$\alpha_S^{\mathrm{cross}} = a_0 + \frac{a_2}{x_T^2} - \frac{a_3}{x_T^3} + \frac{a_4}{x_T^4} + \frac{a_6 \cdot \sigma(\mu_B)}{x_T^6}. \tag{13}$$

Here the coefficients a_i are fixed at $\mu_B = 0$ [where $\sigma(\mu_B = 0) = 1$] by fitting the DQPM coupling constant $g^2(T, \mu_B = 0)$ obtained from Eq. (6) (see the comparison of the basic thermodynamic observables from DQPM-CP and lQCD predictions in Sec. III): $a_0 = 0.25$, $a_2 = 1.77$, $a_3 = 2.17$, $a_4 = 2.13$, $a_6 = 0.85$.

The motivation to use the decrease in the effective coupling is based on the expectations of the QGP matter to approach the noninteracting Stefan-Boltzmann limit at large μ_B on the order of a few GeV and small temperatures $\mu_B \gg T$ (see recent pQCD results on the pressure in Ref. [34]). Therefore, it is reasonable to assume that the coupling constant also decreases at T_c with increasing μ_B. To describe the decrease of the coupling constant near the T_c with μ_B we introduced an additional factor, affecting the region near the phase transition:

$$\sigma(\mu_B) = 1 - \sigma_2 \mu_B^2 - \sigma_4 \mu_B^4, \tag{14}$$

where $\sigma_2 = 0.45$ GeV^{-2} and $\sigma_4 = 0.15$ GeV^{-4}. We fixed the values of σ_2 and σ_4 by fitting the quasiparticle entropy from Eq. (10) to the lQCD data points of the entropy density from the BMW Collaboration [16,17] at finite $\mu_B = 0.1$, 0.2, 0.3, 0.4 GeV for given temperature points $T_c(\mu_B) < T < T_{\mathrm{max}}$, where $T_c(\mu_B)$ denotes the critical temperature and $T_{\mathrm{max}} = 0.4$ GeV.

We note that the adjustment of the effective coupling constant is made in order to interpolate results for thermodynamic observables between the region of vanishing baryon chemical potential and that of the high baryon chemical potential. High and moderate temperatures above the phase transition line $T > T_c(\mu_B)$ are considered. The aim of the model is to describe, on the one side, qualitatively the behavior of the thermodynamic observables in the regions of high/moderate baryon density for $T > T_c(\mu_B)$ and, on the other side, to reproduce the lQCD EoS, the region of moderate baryon chemical potential. For quantitative results, one has to refer to more rigorous approaches. To verify the μ_B dependence of the effective coupling we compare in Fig. 2 the ratio $p/p_{\mathrm{SB}}(T = 0)$ $[p_{\mathrm{SB}}(T = 0) = \frac{\mu_B^4}{108\pi^2}]$ from DQPM-CP calculations for high μ_B with the pQCD calculations from Ref. [34]. Although the uncertainties of the pQCD results are quite large, we see that the resulting pressure from the DQPM-CP is compatible with the pQCD predictions.

Furthermore, to accumulate critical behavior near the CEP, where the phase transition is of second order, we use an additional critical term for the coupling constant. The goal of this term is to describe the critical behavior at the second-order phase transition for the microscopic and thermodynamic quantities. To obtain the parametrization of the critical coupling constant, we fit the entropy density to the results from the PNJL [22]. The resulting parametrization for the critical coupling constant is given by

$$\alpha_S^{\mathrm{crit}} = a \cdot (T/T_c)^{-12}, \tag{15}$$

where $a = \alpha_S^{\mathrm{cross}}(T = T_{\mathrm{CEP}})$.

The total coupling constant $\alpha_S^{\mathrm{DQPM-}CP}$ then reads

$$\alpha_S^{\mathrm{DQPM-}CP} \equiv \begin{cases} \mu_B = \mu_{\mathrm{CEP}} : \alpha_S^{\mathrm{CEP}} = \frac{1-F(T)}{2}\alpha_S^{\mathrm{crit}} + \frac{1+F(T)}{2}\alpha_S^{\mathrm{cross}} \\ \mu_B \neq \mu_{\mathrm{CEP}} : \alpha_S^{\mathrm{cross}} \end{cases} \tag{16}$$

$\alpha_S^{\mathrm{cross}}$ corresponds to the coupling constant for the crossover region defined by Eq. (13), while at $\mu_B = \mu_{\mathrm{CEP}} = 0.960$ GeV the effective coupling $\alpha_S^{\mathrm{DQPM-}CP} = \alpha_S^{\mathrm{CEP}}$

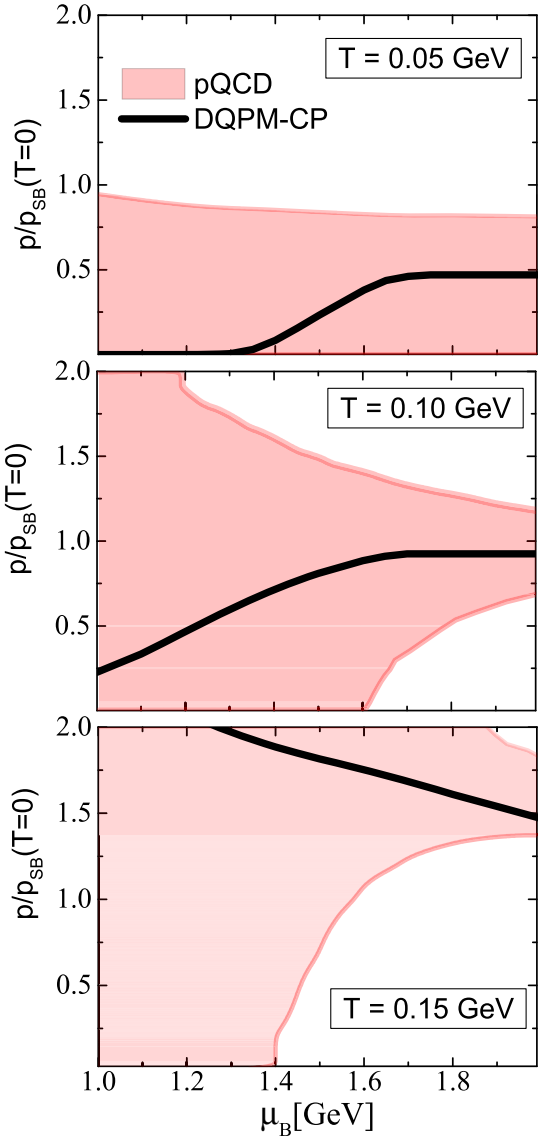

FIG. 2. The scaled pressure p/p_{SB} (black line) from the DQPM-CP in comparison to the pQCD results from Ref. [34] (red area) as a function of the baryon chemical potential for fixed temperatures $T = 0.05$, 0.10, 0.150 GeV. Scenario: $\mu_q = \mu_u = \mu_s = \mu_B/3$.

includes the additional critical ' contribution α_S^{crit}, defined by Eq. (15). To match the two coupling constants we employ the smoothing function:

$$F(T) = \tanh\left[\frac{T - 0.1004}{\delta T}\right], \tag{17}$$

where $\delta T = 0.002$ GeV is the region in the vicinity of the CEP, where the two coupling constants have to match. The values of δT and T are chosen in accordance with the T/T_c—dependence of the PNJL entropy density. While the temperature $T_0 = 0.1004$ GeV regulates the size or temperature range (T_{CEP}, T_0) of the critical contribution, δT affects the derivatives of the pressure at T_0. However, a slight change of T_0 as well as δT up to 20% will not change the qualitative results; the effect of an increase of the second-order derivatives will be less pronounced for smaller T_0.

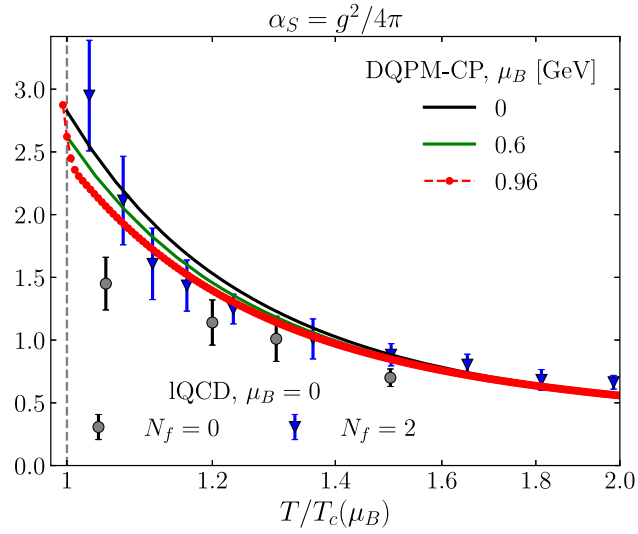

FIG. 3. The running coupling $\alpha_S^{\mathrm{DQPM-}CP}$ from Eq. (16) as a function of the scaled temperature T/T_c at fixed μ_B: for $\mu_{\mathrm{B}} = 0$, $T_c = 0.158$ GeV (black solid line) corresponds to the crossover phase transition and $(T^{\mathrm{CEP}}, \mu_B^{\mathrm{CEP}}) = (0.100, 0.960)$ GeV (red points) corresponds to the CEP. The lattice results for quenched QCD, $N_f = 0$, (black circles) are taken from Ref. [35] and for $N_f = 2$ (blue triangles) are taken from Ref. [36].

Figure 3 shows the effective coupling of the DQPM-CP at fixed $\mu_B = 0$ (black solid line) and $\mu_B = 0.96$ GeV (red points) as a function of the scaled temperature T/T_c. At $\mu_B = 0$ the coupling constant equals the DQPM effective coupling $g^2(T, \mu_{\mathrm{B}} = 0)$ obtained from Eq. (6).

The scaling behavior of the quasiparticle masses has been employed in condensed matter physics [37], where the interaction with bosonic fluctuations near the critical point causes a divergence in the effective masses of the quasiparticles. We note that one can include the scaling behavior of the thermodynamic observables in a more rigorous way as done in Ref. [38], where the EoS from the lQCD calculations of the BMW Collaboration has been parametrized and adopted to include a singular part near the CEP from the 3D-Ising model.

The effective masses (a) and widths (b) of quarks and gluons along the critical line are depicted on Fig. 4. The masses decrease with increasing of μ_B, while at the CEP they show a peak, which corresponds to the finite value of the critical coupling constant. Since the effective masses reflect medium modifications, the increase when approaching the CEP is expected. The thermal widths should accordingly manifest a similar behavior. The widths of the quarks and gluons are significantly smaller then the masses for the whole μ_B range (see Fig. 5). The ratio of the pole mass to the width follows from Eqs. (3)–(5):

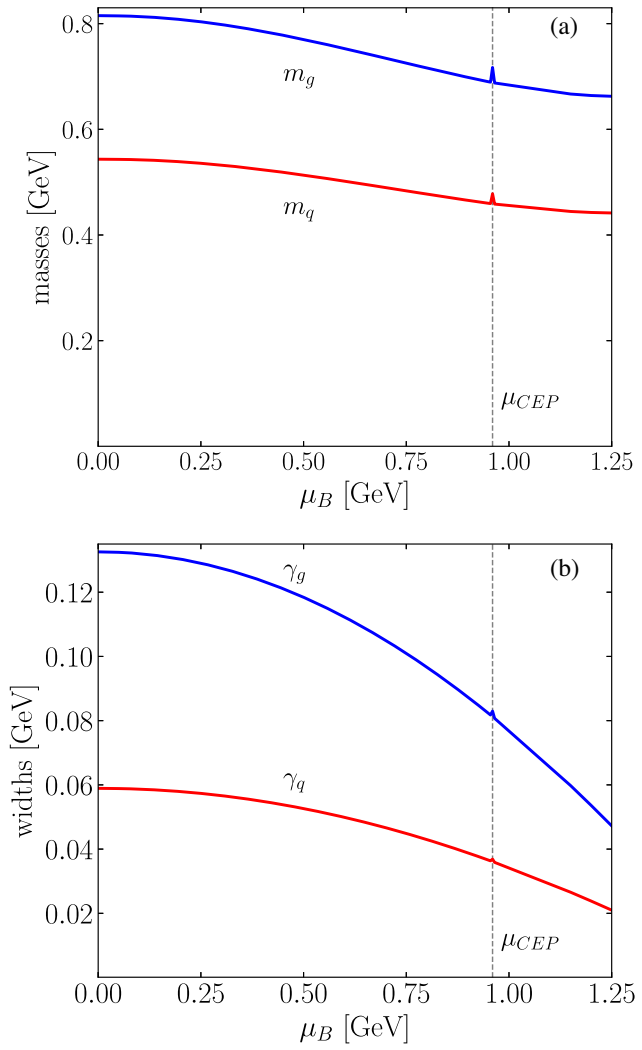

FIG. 4. Effective masses (a) and widths (b) of light quarks and gluons in the DQPM-CP from Eqs. (4)–(5) along the critical line [given by Eq. (12)] as function of baryon chemical potential $\mu_B = 3\mu_q$. The dashed line represents the critical value of the baryon chemical potential $\mu_{\rm CEP} = 0.96$ GeV.

$$m_i/\gamma_i \propto \frac{a_i + b_i \frac{\mu_q^2}{T^2\pi^2}}{g(T,\mu_B)\ln\left(2c_m/g^2(T,\mu_{\rm B})+1\right)}, \qquad (18)$$

where we use the shorthand notation for constants $a_i = 1$ (for quarks), $1 + \frac{N_f}{2N_c}$ (for gluons), $b_i = 1$ (for quarks), and $3/2$ (for gluons). For vanishing chemical potential the ratio $m_i/\gamma_i \approx 9$ for quarks and ≈6 for gluons. The ratio increases with μ_B since the coupling constant decreases with μ_B, for instance at $\mu_B = 1$ GeV: we set $m_i/\gamma_i \approx 16$ for quarks and ≈11 for gluons.

Importantly, we see that in DQPM-CP the quark masses are larger than a third of the free proton mass. This means that the production of baryons across the critical line, the dominant process for large μ_B and small T, is an exothermic process in DQPM-CP.

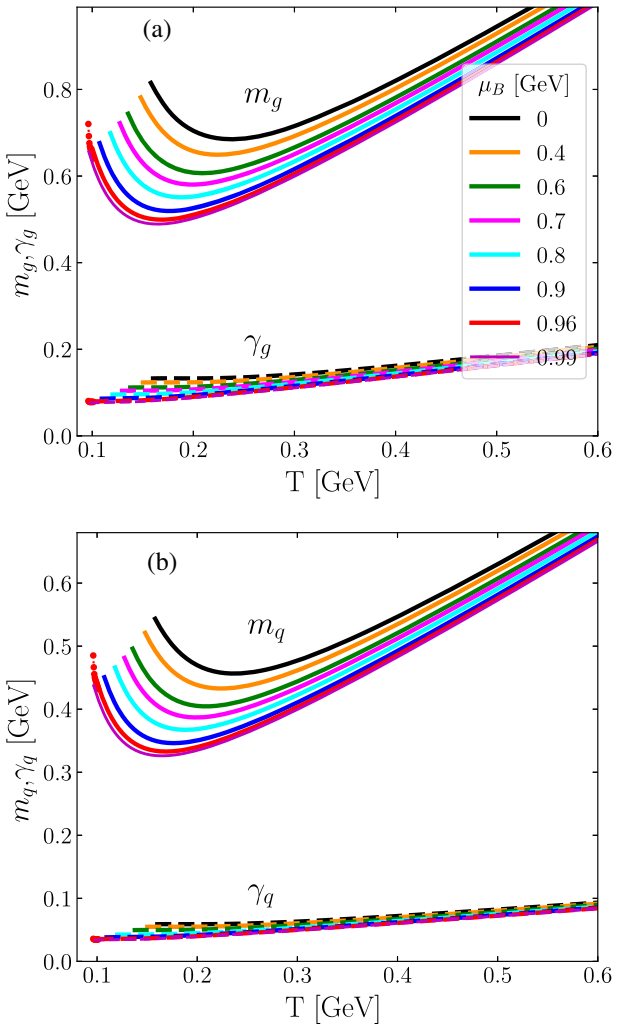

FIG. 5. The DQPM-CP pole masses and widths for the gluons (a) and light quarks (b) given by Eqs. (3)–(5) as a function of temperature in region $T > T_c(\mu_B)$ for fixed baryon potentials $\mu_B \geq 0$.

III. EOS FOR FINITE TEMPERATURE AND CHEMICAL POTENTIAL

In this section we consider the basic thermodynamic observables from the DQPM-CP for finite chemical potential. The starting point for the calculation of the thermodynamic functions in the dynamical quasiparticle models is the evaluation of the entropy density and the quark densities via the propagators as described in Eqs. (10) and (11). Then it is straightforward to derive the pressure p and later the energy density, employing the Maxwell relation for a grand canonical ensemble:

$$p(T,\mu_{\rm B}) = p_0(T,0) + \int_0^{\mu_{\rm B}} n_B(T,\mu'_{\rm B})d\mu'_{\rm B}. \qquad (19)$$

For the pressure at $\mu_B = 0$, we use the lQCD parametrization of the pressure $p_0(T,0)$ from Refs. [16,17]. The energy density ϵ then follows from the Euler relation

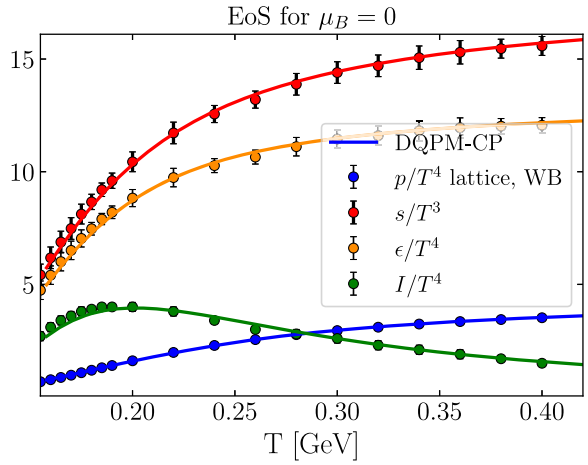

FIG. 6. The scaled pressure $P(T)/T^4$ (blue line), entropy density $s(T)/T^3$ (red line), scaled energy density $\epsilon(T)/T^4$ (orange line), and interaction measure $I(T)/T^4$ (green line), from the DQPM-CP in comparison to the lQCD results from Refs. [16,17] (circles) for zero baryon chemical potential.

$$\epsilon = Ts - p + \sum_i \mu_i n_i. \tag{20}$$

Furthermore, the interaction measure is defined as

$$I \equiv \epsilon - 3P = Ts - 4p + \sum_i \mu_i n_i, \tag{21}$$

which vanishes in the noninteracting limit of massless degrees of freedom at $\mu_B = 0$. The scaled pressure, entropy density, and energy density of the QGP phase are supposed to increase with the temperature. However, lQCD calculations of the thermodynamic observables show [39] that the massless noninteracting limit cannot be reached even at temperatures of $T \sim 1$ GeV. Figure 6 demonstrates thermodynamic observables from the DQPM-CP (solid lines) as a function of temperature at $\mu_B = 0$ in comparison to lQCD data obtained by the BMW Collaboration (dots) [16,17].

We consider two setups for the quark chemical potentials: (I) $\mu_q = \mu_u = \mu_s = \mu_B/3$ and (II) $\mu_s = 0, \mu_u = \mu_B/3$. The quark chemical potential can be related to the strange, baryon, and electric charge chemical potentials as $\mu_i = B_i\mu_B + Q_i\mu_Q + S_i\mu_S$, where B_i,Q_i, and S_i are baryon number, electric charge, and strangeness of the considered quark. Herein we fix $\mu_Q = 0$, therefore for the symmetric QGP matter (I) $\mu_q = \mu_u = \mu_s = \mu_B/3$ the strange and the electric charge potentials are vanishing $\mu_S = \mu_Q = 0$, while for (II) $\mu_s = 0, \mu_u = \mu_B/3$ the strange chemical potential is finite $\mu_S = \mu_B/3$.

The T dependence of the thermodynamic quantities such as the scaled entropy density, the pressure, and the energy density from the DQPM-CP for various baryon chemical potentials $0 \le \mu_B \le 0.99$ GeV is shown in Fig. 7 ($\mu_q = \mu_u = \mu_s = \mu_B/3$) and Fig. 8 ($\mu_s = 0, \mu_u = \mu_B/3$). For setup (I) we found a good agreement between the

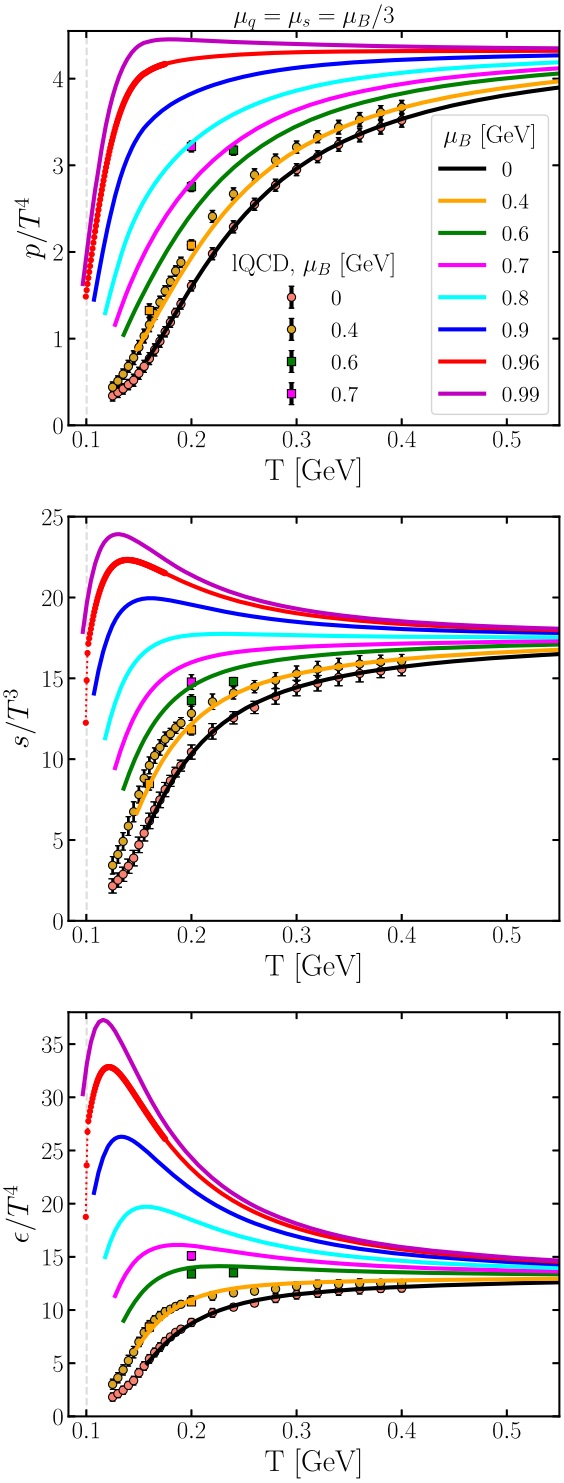

FIG. 7. Scenario: $\mu_q = \mu_u = \mu_s = \mu_B/3$. From top to bottom: Scaled pressure p/T^4, entropy density s/T^3, and scaled energy density ϵ/T^4 from the DQPM (lines) as a function of temperature T at various values of μ_B [GeV]. The lQCD results obtained by the BMW group are taken from Refs. [16,17] (circles) and from Ref. [27] (squares). The dashed line displays the critical temperature $T_{CEP} = 0.10$ GeV.

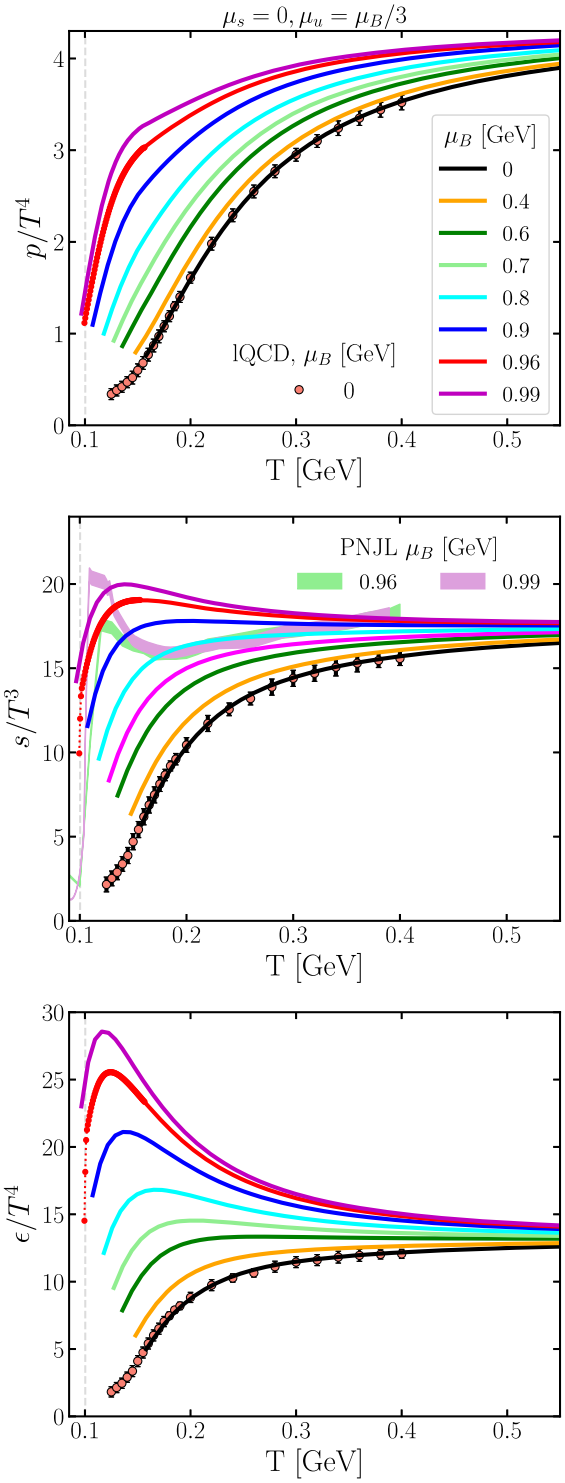

FIG. 8. Scenario: $\mu_s = 0, \mu_u = \mu_B/3$. From top to bottom: Scaled pressure p/T^4, entropy density s/T^3, and scaled energy density ϵ/T^4 from the DQPM-CP (lines) as a function of temperature T at various values of μ_B [GeV]. The lQCD results obtained by the BMW group are taken from Refs. [16,17] (circles). The PNJL results for the entropy density (colored area) are taken from Ref. [22].

DQPM-CP results (lines) and results from lQCD, obtained by the BMW group [16,17] at $\mu_B = 0$ and $\mu_B = 400$ MeV. The thermodynamical quantities increase with μ_B. When approaching the CEP at $\mu_B = 0.96$ GeV the values of the entropy density, of the energy density as well as of the quark or baryon density rise suddenly.

For setup (II) we compare the results for the entropy density to that of the Nantes PNJL approach [22]. The DQPM-CP results are in agreement with the PNJL results in the high-temperature region $T \geq 0.3$ GeV, while in the vicinity of the phase transition there is a clear deviation from the PNJL results, which can be expected since the two models encompass different microscopic properties of the degrees of freedom. The resulting values of the thermodynamic observables for setup (II) is smaller than for setup (I) since the contribution from the strange quarks to the quasiparticle entropy density [see Eq. (10)] is smaller for $\mu_s = 0$ mainly due to the derivatives $\frac{\partial f_q(\omega-\mu_q)}{\partial T}$.

A. Approaching the CEP from the deconfined phase

To realize a critical behavior of the thermodynamic observables in the vicinity of the CEP we introduce, as described in Sec. II B, the critical contribution to the coupling constant that affects the microscopic and macroscopic quantities. At the CEP, where the transition is of second order, the entropy density and baryon density increase rapidly but remain finite, while the quark susceptibility and the specific heat $C_V/T^3 = \frac{d\epsilon}{dT}$ diverge. Therefore, the speed of sound (squared) vanishes as one approaches the CEP. We consider the speed of sound and

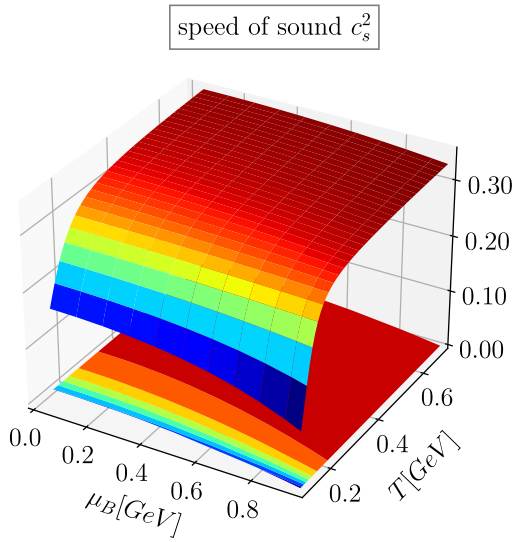

FIG. 9. Scenario: $\mu_q = \mu_u = \mu_s = \mu_B/3$. The speed of sound squared c_s^2 from the DQPM-CP for a crossover phase transition ($0 \leq \mu_B < 0.96$) as a function of T and μ_B.

the specific heat at fixed μ_B. For fixed μ_B the speed of sound can be expressed as

$$c_s^2 = \frac{dp}{d\epsilon} = \frac{dp/dT}{d\epsilon/dT} = \frac{s}{C_V}. \tag{22}$$

The speed of sound squared in the DQPM-CP is depicted in Fig. 9 as a function of temperature T and baryon chemical potential μ_B in the crossover region, where $\mu_B \leq 0.95$ GeV. The resulting c_s^2 increases with temperature and decreases near the phase transition with increasing μ_B. In Fig. 10(a) we show the comparison of the DQPM-CP results for c_s^2 at vanishing μ_B with the available lQCD estimations from the Wuppertal-Budapest Collaboration [17] (light red circles) and the HotQCD Collaboration [26] (blue triangles). The DQPM-CP results are in agreement with the lattice QCD predictions within the estimated errors. Figure 10(b) shows the speed of sound squared c_s^2 from the DQPM-CP as a function of the temperature for a wide range of baryon chemical potentials, including the region of the CEP. At high temperatures, values of c_s^2 are approaching the limit of a noninteracting gas of massless quarks and gluons (SB limit, black dash-dotted line) $c_s^2(\mathrm{SB}) = 1/3$. When increasing the baryon chemical potential the speed of sound near the transition temperature decreases, while at the CEP the speed of sound undergoes a sharp decrease.

The DQPM-CP results for the scaled specific heat C_V/T^3 as a function of T are presented in Fig. 11. As compared to the speed of sound, the specific heat shows an opposite tendency near the phase transition. For moderate values of the baryon chemical potential μ_B the scaled specific heat increases moderately with decreasing temperature. As it approaches the CEP, C_V/T^3 diverges as a function of T, which is consistent with the expectations for a second-order phase transition.

The T dependence of the specific heat for $\mu_B = 0.96$ GeV near the CEP enables us to estimate the value of the critical exponent for $T > T_{\mathrm{CEP}}$:

$$\ln(C_V) = -\alpha \cdot \ln(T - T_{\mathrm{CEP}}) + \mathrm{const}. \tag{23}$$

For the presented parametrization of the coupling constant, we obtain the following values: $\alpha = 0.63 \pm 0.02$ and $\mathrm{const} = -5.48 \pm 0.01$. The value of the critical exponent α is in agreement with the predictions from the PNJL model for $T > T_{\mathrm{CEP}}$ $\alpha_{\mathrm{PNJL}} = 0.68 \pm 0.01$ [31] and the expectations from the universality argument $\alpha = 2/3$ in Ref. [40].

In the case of QCD with finite quark masses, both the chiral and center symmetries are explicitly broken. What remains is the $Z(2)$ sign symmetry of the order parameter

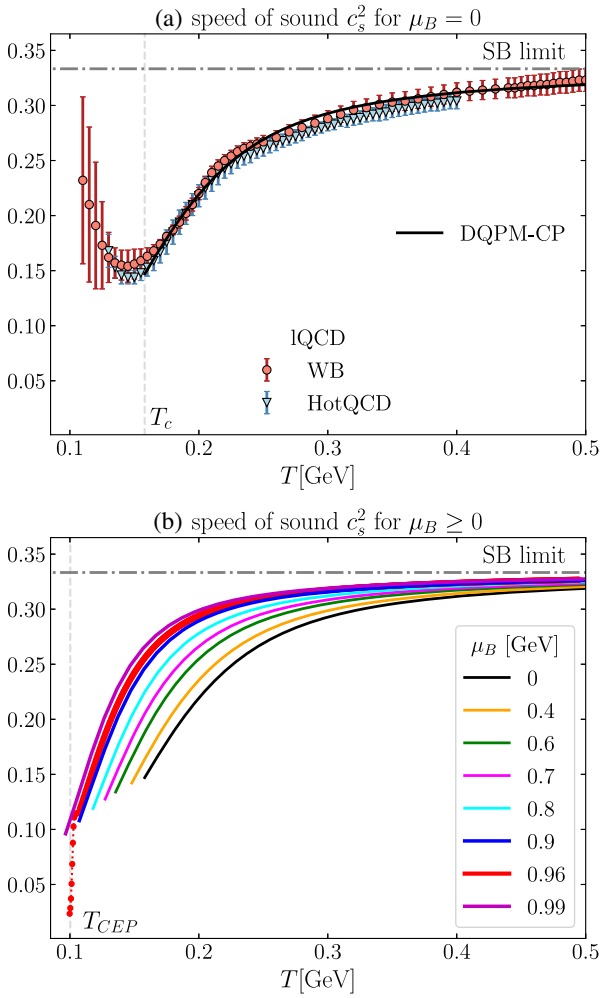

FIG. 10. Scenario: $\mu_q = \mu_u = \mu_s = \mu_B/3$. The speed of sound squared c_s^2 from the DQPM-CP for (a) $\mu_B = 0$ and (b) $\mu_B \geq 0$ as a function of T compared to lQCD results for $\mu_B = 0$ obtained by the Wuppertal-Budapest collaboration [17] (light red circles) and the HotQCD Collaboration [26] (blue triangles).

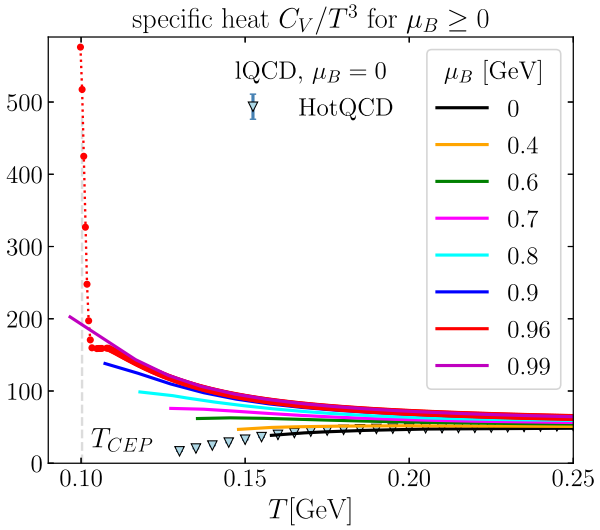

FIG. 11. Scenario: $\mu_q = \mu_u = \mu_s = \mu_B/3$. The specific heat C_V/T^3 from the DQPM-CP at fixed μ_B as a function of T compared to lQCD results for $\mu_B = 0$ of the HotQCD Collaboration [26].

of the chiral phase transition. Therefore it has been assumed that the CEP of QCD with finite quark masses belongs to the three-dimensional $Z(2)$ Ising universality class [41–43]. The corresponding critical exponent in the $Z(2)$ universality class is $\alpha \approx 0.11$ [44]. However, it is known that the critical exponents in the PNJL(NJL) model and $Z(2)$ universality class differ [31,45–48].

To explore the high density region, it is essential for effective models to consider isentropic trajectories for which the ratio of entropy to baryon number is held constant. The isentropic trajectories correspond to the ideal hydrodynamical expansion of QGP matter, created in the HICs. When dissipative effects, which can be described by the viscosities and diffusion coefficients, become important, the trajectories are modified [49,50]. The presence of the CEP can affect the isentropic trajectories, since the entropy density and baryon density undergo a rapid change as the phase transition is approached. It is supposed that the CEP acts as an attractor of isentropic trajectories [51]. Moreover, a different choice for the strange quark chemical potential affects the trajectories as well. Therefore we compare the resulting isentropic trajectories for two setups of the strange chemical potential.

Figure 12 displays the isentropic trajectories from the DQPM-CP for (a) $\mu_q = \mu_s = \mu_u = \mu_B/3$ and (b) $\mu_s = 0$, $\mu_u = \mu_d = \mu_B/3$ in the phase diagram. Comparing (a) to (b), one can clearly see that the trajectories for the zero strange quark chemical potential are shifted towards higher μ_B values. In the case of vanishing chemical potential of the strange quark $\mu_s = 0, \mu_u = \mu_d = \mu_B/3$, the entropy density, which has also contributions from the light (anti-)quarks and gluons, is less affected then the baryon density. Therefore, for finite $\mu_B > 0$ and $\mu_s = 0$, the ratio s/n_B is larger than in the case of a symmetric setup $\mu_s = \mu_u = \mu_B/3$ and the value of the baryon density decreases faster than the entropy density. This observation is in agreement with previous studies of the PNJL model [33] and the results from Refs. [38,52], where the lQCD EoS from the WB Collaboration [16,17,53] with a critical point in the 3D Ising model universality class is considered for moderate baryon chemical potentials $\mu_B \leq 0.45$ GeV. Thus, a critical trajectory, which goes through the CEP, for (a) corresponds to $s/n_B \approx 13.35$ and for (b) corresponds to $s/n_B \approx 15$. The comparison of isentropic trajectories in a vicinity of the CEP is presented in Fig. 12(c). In the vicinity of the CEP, the trajectories with $s/n_B = 15, 13.35, 12$ shown in Fig. 12(c) are focused to the critical endpoint.

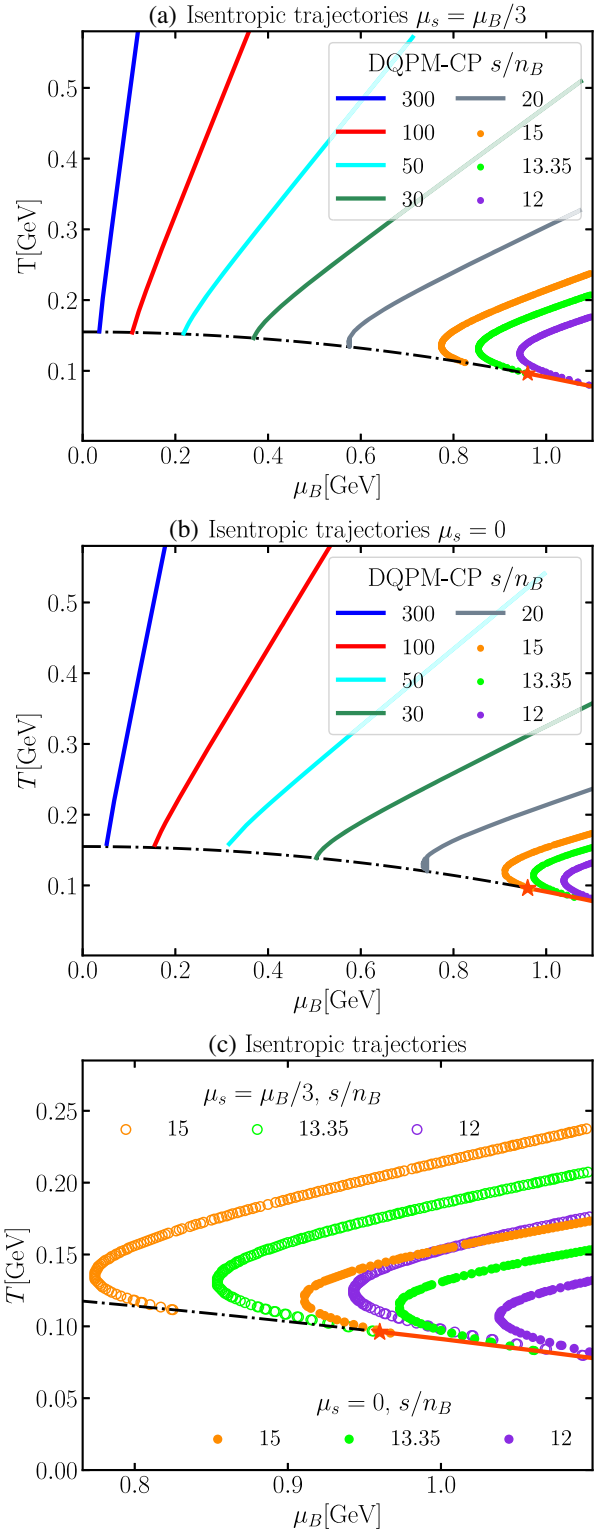

FIG. 12. Trajectories of constant s/n_B in the DQPM-CP phase diagram for $T > T_c$ and (a) $\mu_q = \mu_u = \mu_s = \mu_B/3$, (b) $\mu_s = 0, \mu_u = \mu_B/3$, and (c) two cases in the vicinity of the critical endpoint CEP. The finite temperature crossover (black dash-dotted line) at small chemical potential switches to the large chemical potential first-order transition (red solid line) at the CEP (star), which is located at (0.10,0.96) GeV.

IV. TRANSPORT COEFFICIENTS

We continue to investigate the transport properties of QGP matter using the DQPM-CP. We consider the specific shear η/s and bulk ζ/s viscosities, the ratio of electric σ_{QQ}/T, baryon σ_{BB}/T, and strange σ_{SS}/T conductivities to

temperature. At vanishing baryon chemical potential, the DQPM-CP model equals the DQPM; therefore, one can find the comparison of DQPM transport coefficients at $\mu_B = 0$ with the recent results from various approaches in previous papers [6,54,55].

All transport coefficients are calculated within the relaxation time approximation (RTA) of the Boltzmann equation. In the relaxation time approximation (in first order in the deviation from equilibrium) the collision term is given by [56]

$$\sum_{j=1}^{N_{\text{species}}} C_{ij}^{(1)}[f_i] = -\frac{E_i}{\tau_i}(f_i - f_i^{(0)}) = -\frac{E_i}{\tau_i} f_i^{(1)} + \mathcal{O}(\text{Kn}^2), \tag{24}$$

where τ_i is the relaxation time in the heat bath rest system for the particle species $'i'$, and $\text{Kn} \sim l_{\text{micro}}/L_{\text{macro}}$ is the Knudsen number which denotes the ratio between the relevant microscopic scale (mean free path) over the characteristic length scale of the system. The equilibrium state of the system is described by the Bose-Einstein and Fermi-Dirac distribution functions

$$f_i^{(0)}(E_i, T, \mu_i) = \frac{1}{\exp\left((E_i - \mu_i)/T\right) - a_i}, \tag{25}$$

where μ_i is the quark chemical potential, $E_i = \sqrt{\mathbf{p}_i^2 + m_i^2}$ is the on-shell quark/gluon energy, and $a_i \equiv +1(\text{gluons}), -1((\text{anti-})\text{quark})$. In Eq. (24), $f_i^{(1)}(x,k,t)$ contains $\delta f_i(x,k,t)$, which is the nonequilibrium part to first order in gradients. The first step in the calculation of the transport coefficients within the RTA framework is the estimation of relaxation times, which are supposed to depend on the momentum of the partons, on the temperature and on the baryon chemical potential.

The momentum dependent relaxation time can be expressed through the on-shell interaction rate in the rest system of the medium, in which the incoming quark has a four-momentum $P_i = (E_i, \mathbf{p}_i)$:

$$\begin{aligned}\tau_i^{-1}(p_i, T, \mu_q) &= \Gamma_i(p_i, T, \mu_q) \\ &= \frac{1}{2E_i}\sum_{j=q,\bar{q},g}\frac{1}{1+\delta_{cd}}\int\frac{\mathrm{d}^3 p_j}{(2\pi)^3 2E_j} d_q f_j^{(0)}(E_j, T, \mu_q) \\ &\times \int\frac{\mathrm{d}^3 p_c}{(2\pi)^3 2E_c}\int\frac{\mathrm{d}^3 p_d}{(2\pi)^3 2E_d}|\bar{\mathcal{M}}|^2(p_i, p_j, p_c, p_d)(2\pi)^4 \\ &\times \delta^{(4)}(p_i + p_j - p_c - p_d)(1 - f_c^{(0)})(1 - f_d^{(0)}),\end{aligned} \tag{26}$$

where $|\bar{\mathcal{M}}|^2$ denotes the matrix element squared averaged over the color and spin of the incoming partons, and summed over those of the final partons. The $|\bar{\mathcal{M}}|^2$ is calculated by the use of the effective coupling and propagators in leading order (for further details see [6]). The notation $\sum_{j=q,\bar{q},g}$ includes the contribution from all possible partons which in our case are the gluons and the (anti-)quarks of three different flavors (u, d, s). The quark relaxation time is expected to become very large near CEP, since the correlation length increases rapidly close to the CEP.

A. Specific viscosities

We start with the most common transport coefficients for the hydrodynamical simulations—the shear and bulk viscosity. The viscosities of the QCD matter have been studied within a variety models in the confined and the deconfined phases. The shear viscosity reveals the strength of the interaction inside the QCD medium, in particular, within the kinetic theory it can be related to the hadron or parton interaction rates, which is a challenge to evaluate on the basis of first principles. A plethora of theoretical model predictions show that the temperature dependence of the QCD shear viscosity over entropy density η/s is qualitatively different for the two phases. Starting from the hadronic phase below the phase transition $T < T_c$, η/s monotonically decreases with T since the system is dominated by pions with weaker interactions at lower T. While above the phase transition $T > T_c$, η/s increases with temperature because the interaction attenuates at high T. Approaching the phase transition from hadronic to the QGP phase at vanishing chemical potential, η/s has a wide dip followed by an increase with temperature. A similar property of the temperature dependence of the specific shear viscosity η/s is seen for other fluids such as H_2O, He, and N_2 [57–59]. The specific bulk viscosity of the QGP matter is predicted to be low, yet it is expected to be finite near the phase transition [60]. The presence of the bulk viscosity reduces the speed of the fluid radial expansion and hence affects the mean momentum of the produced particles. For conformal fluids, the bulk viscosity is known to be identically zero, and the deconfined QCD medium is expected to adopt a conformal behavior in the high-energy or temperature regime. Nevertheless, the lQCD results on the enhanced trace anomaly close to T_c have shown that it is probably not the case for the deconfined QCD medium in the vicinity of the phase transition.

The shear and bulk viscosity for quasiparticles with medium-dependent masses $m_i(T, \mu_q)$ can be derived using the Boltzmann equation in the RTA [61] through the relaxation time:

$$\begin{aligned}\eta(T, \mu_q) = \frac{1}{15T}\sum_{i=q,\bar{q},g}\int\frac{d^3 p}{(2\pi)^3}\frac{\mathbf{p}^4}{E_i^2}\tau_i(\mathbf{p}, T, \mu_q) \\ \times d_i(1 \pm f_i) f_i,\end{aligned} \tag{27}$$

$$\zeta(T,\mu_q) = \frac{1}{9T}\sum_{i=q,\bar{q},g}\int\frac{d^3p}{(2\pi)^3}\tau_i(\mathbf{p},T,\mu_q)\frac{d_i(1\pm f_i)f_i}{E_i^2} \times\left[\mathbf{p}^2 - 3c_s^2\left(E_i^2 - T^2\frac{dm_i^2}{dT^2}\right)\right]^2, \quad (28)$$

where $q(\bar{q}) = u, d, s(\bar{u}, \bar{d}, \bar{s})$, $d_q = 2N_c = 6$, and $d_g = 2(N_c^2 - 1) = 16$ are the degeneracy factors for spin and color for quarks and gluons, respectively, τ_i are the relaxation times, c_s is the speed of sound for a fixed μ_B given by Eq. (22), and $\frac{dm_i^2}{dT^2}$ is the derivative of the effective masses. As it was shown in the previous studies [6,32,55,62,63] in the case of the medium-dependent masses, the viscosities display a pronounced temperature behavior. At vanishing baryon chemical potential we found previously that the DQPM results for specific shear and bulk viscosity [6,54] are very close to the predictions from the gluodynamic lQCD calculations [64,65].

For moderate values of the baryon chemical potential, the specific shear viscosity η/s of the QGP matter increases with temperature, while the specific bulk viscosity ζ/s decreases with temperature, independent of baryon chemical potential. However, the T dependence of η/s near the phase transition changes with increasing μ_B. Figure 13 shows the DQPM-CP results for η/s as a function of scaled temperature $T/T_c(\mu_B)$, for different μ_B values. The specific shear viscosity for $\mu_B = 0$ (red line) shows a dip followed by an increase with temperature while for a $\mu_B \geq 0.9$ GeV η/s decreases with increasing temperature near the phase transition ($T \leq 2T_c$). The parton relaxation time τ_i decreases with increasing temperature at lower T, and remains approximately constant at high T for moderate values of chemical potential $\mu_B \geq 0.6$ GeV. Therefore the shear viscosity $\eta \sim T^4$, while the entropy density grows as $s \sim T^3$. Thus, in the high-temperature region the ratio η/s increases as $\sim T$. It is important to note that transport coefficients rely on the microscopic properties of the degrees of freedom. While a variety of the models can reproduce the lQCD results of basic thermodynamic observables, the transport coefficients differ between the models.

Here we compare results of the specific shear viscosity and later of the electric conductivity for nonzero baryon or quark chemical potential with the RTA results from the PNJL model for $\mu_s = 0, \mu_u = \mu_B/3$ in Fig. 13(a). The specific shear viscosity results from the DQPM-CP (solid lines) for $\mu_B = 0$, 0.6 GeV agree well with the predictions of the PNJL model (dashed lines) in the vicinity of the phase transition for temperatures $T \leq 1.5T_c$. The DQPM-CP results for η/s at $\mu_B = 0.96$ GeV for $T \leq 2T_c$ is higher than from the PNJL model, while the temperature dependence is similar. The discrepancy between the results is caused by the different treatment of the gluonic degrees of freedom, which has a pronounced critical behavior of the

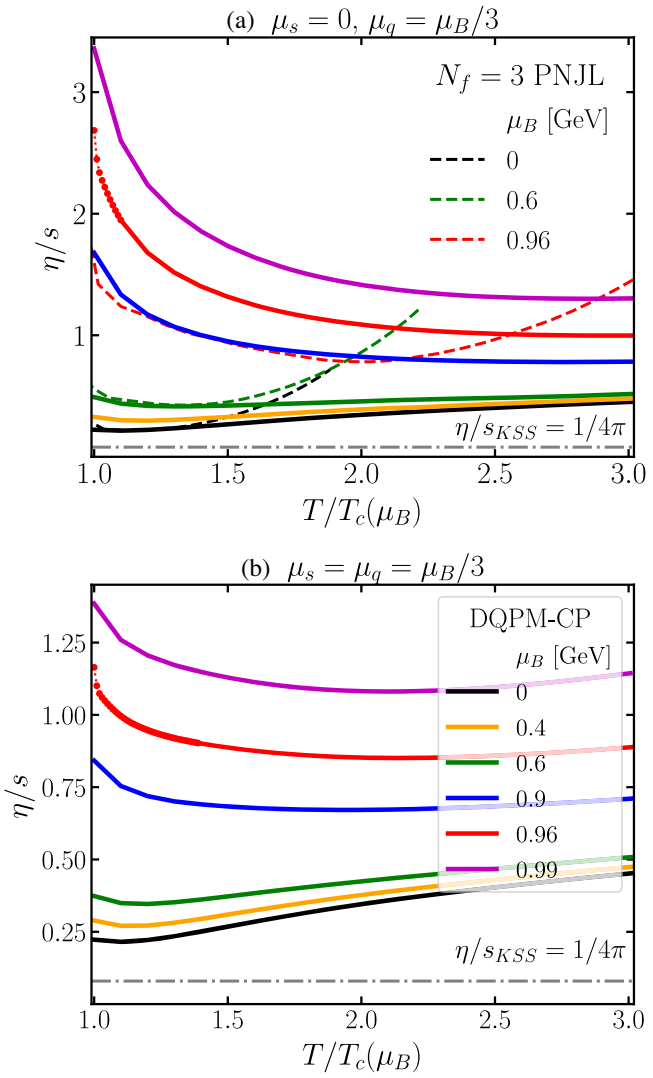

FIG. 13. Specific shear η/s viscosity from the DQPM-CP (solid lines) for two setups of strange chemical potential: (a) ($\mu_s = 0, \mu_u = \mu_B/3$) and (b) ($\mu_s = \mu_u = \mu_B/3$) as a function of the scaled temperature T/T_c for various $\mu_B \geq 0$. We compare to the RTA estimates from the $N_f = 3$ PNJL model (dashed lines) [54]. The grey dashed-dotted line demonstrates the Kovtun-Son-Starinets bound [66] $(\eta/s)_{\mathrm{KSS}} = 1/(4\pi)$.

thermal masses in the DQPM-CP model. Increasing the baryon chemical potential, one can see not only an increase in magnitude but also a change in the T dependence of η/s and ζ/s as shown in Figs. 13 and 14. In particular, in the vicinity of the phase transition $T < 1.5T_c$ for moderate values of μ_q the specific shear viscosity shows a dip after the phase transition, which is vanishing at high values of μ_B as can be seen in Fig. 13. As pointed out in Refs. [32,67–69] in the vicinity of the CEP, the divergences of bulk and shear viscosities of the QCD matter are determined by the dynamic and the static critical exponents. The dynamical universality class of the QCD critical

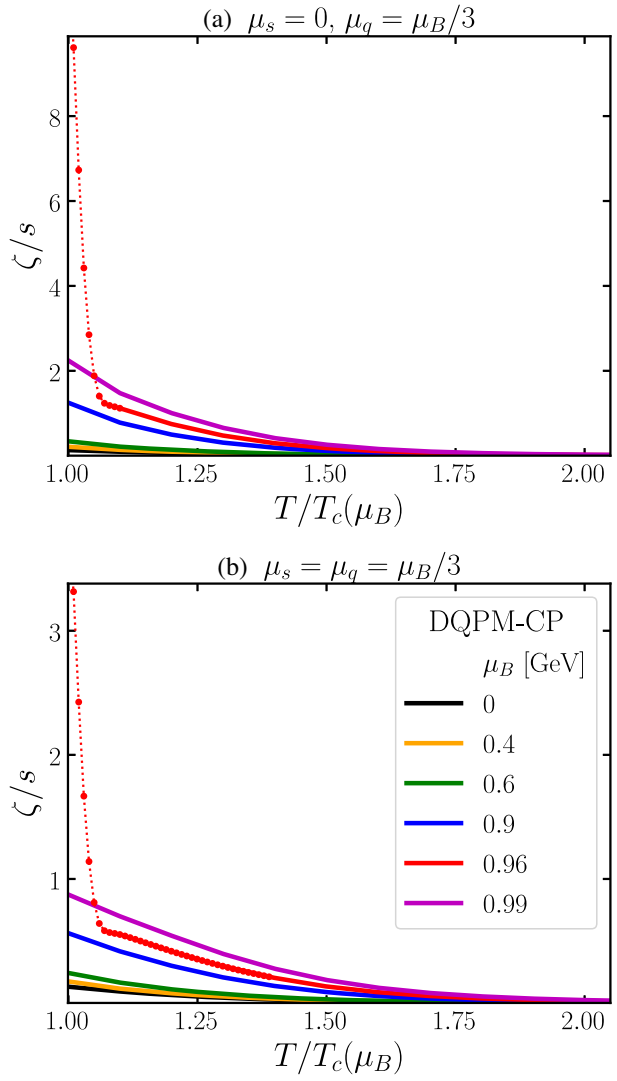

FIG. 14. Specific bulk ζ/s viscosity from the DQPM-CP (solid lines) for two setups of strange chemical potential: (a) $(\mu_s = 0, \mu_u = \mu_B/3)$ and (b) $(\mu_s = \mu_u = \mu_B/3)$ as a function of the scaled temperature T/T_c for various $\mu_B \geq 0$.

endpoint is argued to be that of the H model [67,70] according to the classification of dynamical critical phenomena by Hohenberg and Halperin [71]. Whereas in the vicinity of the CEP the shear viscosity has a mild divergence in the critical region, the bulk viscosity has a more pronounced divergence [67,71,72]: $\eta \sim \xi_T^{Z_\eta}(Z_\eta \approx 1/19)$, $\zeta \sim \xi_T^{Z_\zeta}(Z_\zeta \approx 3)$. The thermal correlation length is controlled by the static critical exponent $\xi_T \sim t^{-\nu}$, $t = \frac{T-T_c}{T_c}$, with ν being the static critical exponent. Using the hyperscaling relation [73] for the static critical exponents we can estimate ν:

$$2 - \alpha = d\nu, \tag{29}$$

where $d = 3$ denotes the number of the spatial dimensions, $\alpha \approx 0.63$. We obtain $\nu \approx 0.46$. Taking into account the dynamical and static exponents, the divergence of the bulk viscosity is assumed to be $\zeta \approx t^{-Z_\zeta \nu + \alpha}$ [69,72,74].

Here we consider small deviations from equilibrium where the quark relaxation times are not large: τ_q is about $4.5 - 2.5$ fm/c for the temperature range $T_c < T \leq 2T_c$, so that the slight divergence of the transport coefficients near the CEP is determined by the static exponents. The specific shear and bulk viscosities from the DQPM-CP increase rapidly when approaching the critical endpoint from the partonic phase. However, the increase near the CEP is more pronounced for the specific bulk viscosity which rises by a factor of five, while the specific shear viscosity rises only by $\lesssim 10\%$ for the same temperature range 1.07–1.01 T/T_c. The increase of ζ/s is related to the rapid decrease in the speed of sound and corresponds to the static critical exponents, which affects the bulk viscosity. In terms of heavy-ion collisions observables, this increase in the bulk viscosity is expected to show up as the decrease of average transverse momentum of produced particles as well as in an increase of the charged particle multiplicity per unit momentum rapidity [60,68]. However, this has to be checked by a transport simulations or by a hydrodynamical simulation of the expanding QGP. Such a substantial increase of the charged particle and net-baryon multiplicities per unit momentum rapidity due to the enhancement of the bulk viscosity near the CEP has been observed in a longitudinally expanding $1 + 1$ dimensional causal relativistic hydrodynamical evolution at nonzero baryon density [75].

We note that the specific bulk and shear viscosities have been considered near the CEP and the first-order phase transition for the $N_f = 2$ NJL model in the previous study [32]. We found good qualitative agreement for the T dependence of the shear and bulk viscosity of the NJL model from Ref. [32], while the numerical values differ due to the different quark relaxation times and the absence of gluonic degrees of freedom in the case of the NJL model.

B. Electric, baryon, and strange conductivities

In the region of the high net baryon density it is important to take into account the diffusion of conserved charges, i.e., electric, baryon and strange charges, from higher density regions to lower density regions. The transport coefficient, which characterizes the diffusion, is the diffusion coefficient κ_q or the conductivity $\sigma_q = \kappa_q/T$ of the conserved charge q. Furthermore, since the quarks carry multiple conserved charges, one needs to consider additionally nondiagonal conductivities for two conserved charges qq'—$\sigma_{qq'}$. Conductivities $\sigma_{qq'}$ for a quasiparticles can be expressed in the RTA [76] as

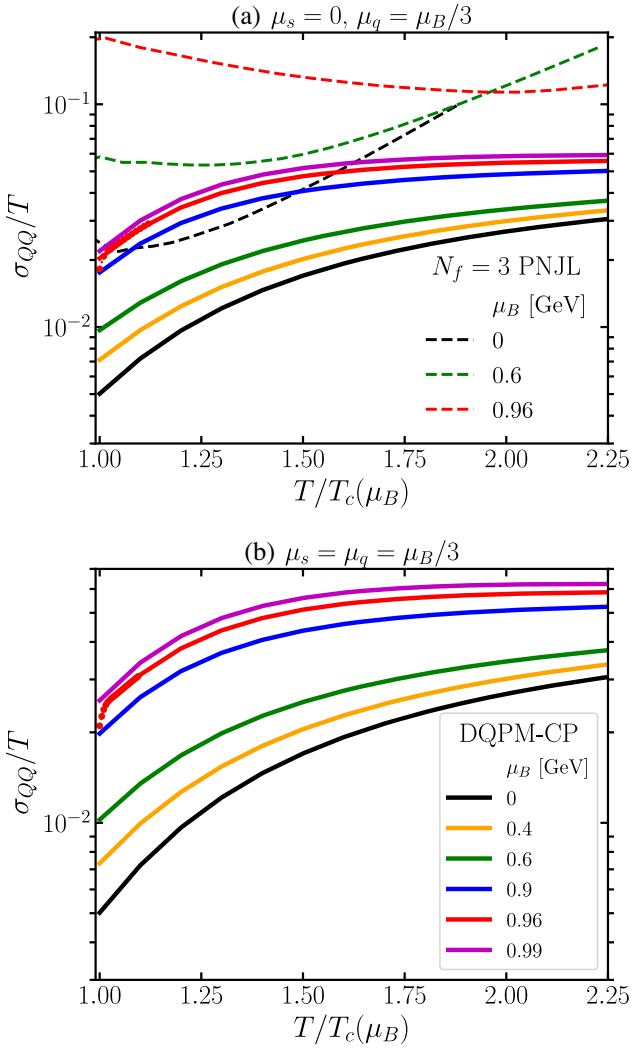

FIG. 15. Scaled electric conductivity as a function of the scaled temperature T/T_c from the DQPM-CP (solid lines) for two setups of strange chemical potential: (a) ($\mu_s = 0, \mu_u = \mu_B/3$) and (b) ($\mu_s = \mu_u = \mu_B/3$) as a function of the scaled temperature T/T_c for various $\mu_B \geq 0$. For ($\mu_s = 0, \mu_u = \mu_B/3$) we compare σ_{QQ}/T from DQPM-CP to the RTA estimates from the $N_f = 3$ PNJL model (dashed lines) [54].

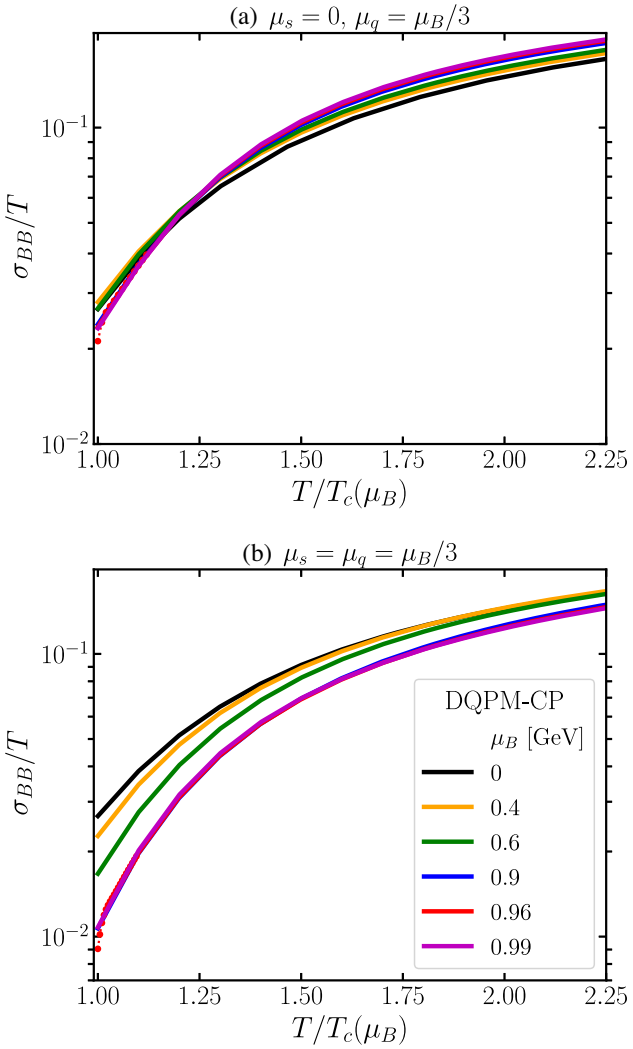

FIG. 16. Scaled baryon conductivity as a function of scaled temperature T/T_c from the DQPM-CP (solid lines) for two setups of strange chemical potential: (a) ($\mu_s = 0, \mu_u = \mu_B/3$) and (b) ($\mu_s = \mu_u = \mu_B/3$) as a function of the scaled temperature T/T_c for various $\mu_B \geq 0$.

$$\sigma qq'(T,\mu_q) = \frac{1}{3T}\sum_{i=q,\bar{q}} q_i \int \frac{d^3p}{(2\pi)^3}\frac{\mathbf{p}^2}{E_i^2}\tau_i(\mathbf{p},T,\mu_q) \times \left(\frac{E_i n_{q'}}{\epsilon + p} - q_i'\right) d_i(1 \pm f_i) f_i. \quad (30)$$

Let us consider first the diagonal conductivities for electric, baryon, and strange charges. The DQPM-CP results for σ_{QQ}/T, σ_{BB}/T and σ_{SS}/T are shown in Figs. 15, 16, 17 as a function of the scaled temperature T/T_c for two setups of the strange quark chemical potential. The scaled electric, strange, and baryon conductivities have a similar temperature dependence: at high T the ratios increase with temperature increase as $\sim T$ which is mainly due to the quark density increasing with temperature. The most prominent difference between the conductivities is the μ_B dependence, which is shown in Figs. 15, 16, and 17: the electric and strange conductivities increase with μ_B, while the baryon conductivity decreases with μ_B for the symmetric setup $\mu_s = \mu_u = \mu_B/3$. With the increase of baryon chemical potential the net baryon density increases, which influences the baryon conductivity. A similar trend for the σ_{QQ}/T, σ_{BB}/T, and σ_{SS}/T at moderate values of baryon chemical potential $\mu_B \leq 0.4$ GeV has been observed in the nonconformal Einstein-Maxwell-Dilaton holographic model [77]. Furthermore, we compare the μ_B dependencies of the scaled conductivities for the two setups of the strange quark chemical potential. We have found that in case of vanishing strange quark chemical potential [setup (II)] the scaled conductivities show a much less pronounced of μ_B dependence for the baryon and strange

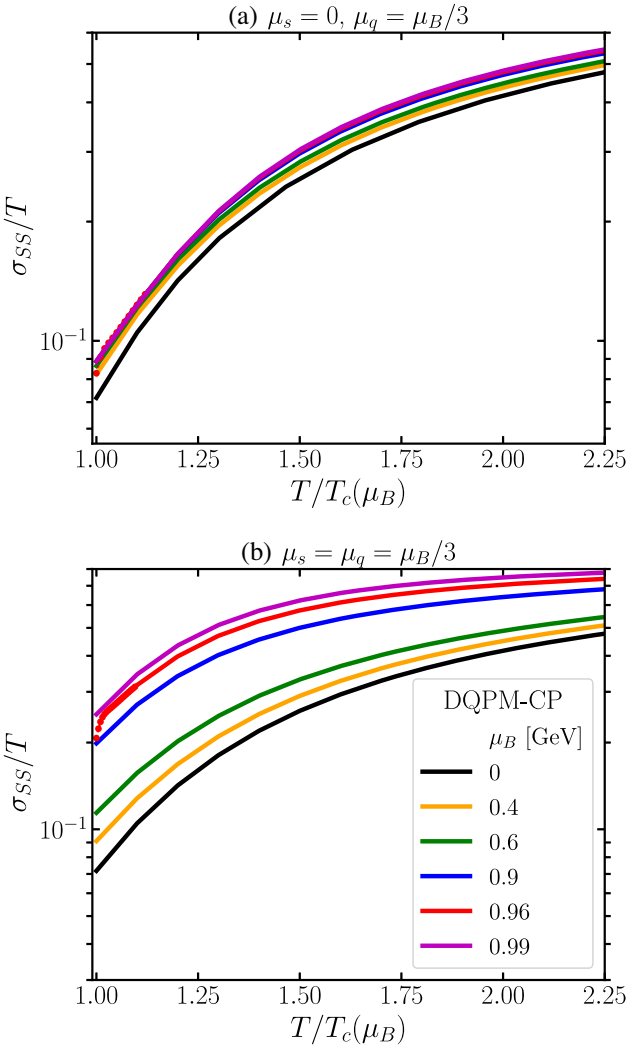

FIG. 17. Scaled strange conductivity as a function of scaled temperature T/T_c from the DQPM-CP (solid lines) for two setups of strange chemical potential: (a) ($\mu_s = 0, \mu_u = \mu_B/3$) and (b) ($\mu_s = \mu_u = \mu_B/3$) as a function of the scaled temperature T/T_c for various $\mu_B \geq 0$.

conductivities, which is expected due to the vanishing net strangeness density $n_S = 0$. Meanwhile the electric conductivity has a similar μ_B dependence for the two settings of strange quark chemical potential. Near the CEP, the electric conductivity decreases, but as for the PNJL results, there is no pronounced divergence behavior. The same behavior has been found for the baryon and strange conductivities.

V. CONCLUSIONS AND OUTLOOK

By extending the phenomenological dynamical quasiparticle model to a wide range of baryon chemical potentials, we obtain an EoS, which is in agreement with the lattice data at moderate baryon chemical potentials and can at the same time be extended to the whole (T, μ_B) plane. This extension allows for calculating the transport coefficients of the partonic phase. To mimic the T dependence of the basic thermodynamic observables near the CEP we have adopted the critical behavior of the effective coupling constant by using the entropy density from the PNJL model near the CEP. For moderate values of the chemical potential $\mu_B \leq 0.4$ GeV the dependence of the thermodynamic quantities on μ_B are in agreement with the previous results from the DQPM [6,15,78].

(i) We presented the results for the thermodynamic observables p/T^4, ϵ/T^4, s/T^3, as well as for the speed of sound and the specific heat for a wide range of chemical potentials. We have shown that the critical behavior of the effective coupling affects the thermodynamic observables. Moreover, we have found that the resulting value of the critical exponent $\alpha \approx 0.63$ is in good agreement with the predictions of the PNJL model and the expectations from the universality argument $\alpha = 2/3$.

(ii) To quantify the μ_B dependence of the bulk observables we have studied isentropic trajectories of the deconfined QCD medium described by the DQPM-CP for a wide range of baryon chemical potential, including the vicinity of the CEP.

(iii) We have evaluated transport properties of the deconfined QCD medium for a wide range of baryon chemical potential within the DQPM-CP: the specific shear η/s and bulk ζ/s viscosity and the ratio of electric σ_{QQ}/T, baryon σ_{BB}/T, and strange σ_{SS}/T conductivities to temperature on the basis of the Boltzmann equation in the relaxation time approximation. We have found that the resulting μ_B dependence of η/s and σ_{QQ}/T for the PNJL model and the DQPM-CP are qualitatively the same in the vicinity of the phase transition, while there is a clear difference in the electric conductivity.

(iv) We have found that the DQPM-CP estimates of the specific bulk viscosity show a rapid increase when approaching the CEP from the high-temperature region originating from the rapid decrease of the speed of sound $c_s^2 \to 0$, whereas for the specific shear viscosity and the B, Q, S conductivities there is only a small enhancement $\leq$10%, caused mainly by the critical contribution of the effective coupling constant.

Although the extracted results for the transport coefficients are model dependent, the qualitative picture of the T and μ_B dependence is consistent with expectations from more rigorous approaches. Our results can be implemented in hydrodynamic simulations as well as be employed for the partonic phase of transport approaches.

ACKNOWLEDGMENTS

The authors thank Wolfgang Cassing, Juan Torres-Rincon, Claudia Ratti. and Taesoo Song for useful discussions. O. S. acknowledge support from the

"Helmholtz Graduate School for Heavy Ion research." O. S. and E. B. acknowledge support by the Deutsche Forschungsgemeinschaft (DFG, German Research Foundation) through the CRC-TR 211 "Strong-interaction matter under extreme conditions" - Project No. 315477589 —TRR 211. This work is supported by the European Union's Horizon 2020 research and innovation program under Grant agreement No. 824093 (STRONG-2020) and by the COST Action THOR, CA15213. Computational resources were provided by the Center for Scientific Computing (CSC) of the Goethe University.

[1] X. An *et al.*, Nucl. Phys. **A1017**, 122343 (2022).
[2] C. S. Fischer, Prog. Part. Nucl. Phys. **105**, 1 (2019).
[3] J. Braun, W.-j. Fu, J. M. Pawlowski, F. Rennecke, D. Rosenblüh, and S. Yin, Phys. Rev. D **102**, 056010 (2020).
[4] J. Ghiglieri, A. Kurkela, M. Strickland, and A. Vuorinen, Phys. Rep. **880**, 1 (2020).
[5] W. Cassing and E. L. Bratkovskaya, Nucl. Phys. **A831**, 215 (2009).
[6] P. Moreau, O. Soloveva, L. Oliva, T. Song, W. Cassing, and E. Bratkovskaya, Phys. Rev. C **100**, 014911 (2019).
[7] S. Plumari, W. M. Alberico, V. Greco, and C. Ratti, Phys. Rev. D **84**, 094004 (2011).
[8] F. Scardina, S. K. Das, V. Minissale, S. Plumari, and V. Greco, Phys. Rev. C **96**, 044905 (2017).
[9] K.-J. Sun, C. M. Ko, and Z.-W. Lin, Phys. Rev. C **103**, 064909 (2021).
[10] A. Peshier and W. Cassing, Phys. Rev. Lett. **94**, 172301 (2005).
[11] W. Cassing, Nucl. Phys. **A795**, 70 (2007).
[12] W. Cassing, Nucl. Phys. **A791**, 365 (2007).
[13] M. L. Bellac, *Thermal Field Theory*, Cambridge Monographs on Mathematical Physics (Cambridge University Press, Cambridge, England, 2011).
[14] O. Linnyk, E. Bratkovskaya, and W. Cassing, Prog. Part. Nucl. Phys. **87**, 50 (2016).
[15] H. Berrehrah, E. Bratkovskaya, T. Steinert, and W. Cassing, Int. J. Mod. Phys. E **25**, 1642003 (2016).
[16] S. Borsanyi, G. Endrodi, Z. Fodor, S. D. Katz, S. Krieg, C. Ratti, and K. K. Szabo, J. High Energy Phys. 08 (2012) 053.
[17] S. Borsanyi, Z. Fodor, C. Hoelbling, S. D. Katz, S. Krieg, and K. K. Szabo, Phys. Lett. B **730**, 99 (2014).
[18] B. Vanderheyden and G. Baym, J. Stat. Phys. **93**, 843 (1998).
[19] J. P. Blaizot, E. Iancu, and A. Rebhan, Phys. Rev. D **63**, 065003 (2001).
[20] S. Borsanyi, Z. Fodor, J. N. Guenther, R. Kara, S. D. Katz, P. Parotto, A. Pasztor, C. Ratti, and K. K. Szabo, Phys. Rev. Lett. **125**, 052001 (2020).
[21] A. Bazavov *et al.* (HotQCD Collaboration), Phys. Lett. B **795**, 15 (2019).
[22] D. Fuseau, T. Steinert, and J. Aichelin, Phys. Rev. C **101**, 065203 (2020).
[23] P. Cea, L. Cosmai, and A. Papa, Phys. Rev. D **93**, 014507 (2016).
[24] M. A. Stephanov, Prog. Theor. Phys. Suppl. **153**, 139 (2004).
[25] J. N. Guenther, arXiv:2201.02072.
[26] A. Bazavov *et al.* (HotQCD Collaboration), Phys. Rev. D **90**, 094503 (2014).
[27] S. Borsányi, Z. Fodor, J. N. Guenther, R. Kara, S. D. Katz, P. Parotto, A. Pásztor, C. Ratti, and K. K. Szabó, Phys. Rev. Lett. **126**, 232001 (2021).
[28] F. Karsch, Proc. Sci., CORFU2018 (2019) 163 [arXiv:1905.03936].
[29] H. T. Ding *et al.* (HotQCD Collaboration), Phys. Rev. Lett. **123**, 062002 (2019).
[30] V. V. Braguta, M. N. Chernodub, A. Y. Kotov, A. V. Molochkov, and A. A. Nikolaev, Phys. Rev. D **100**, 114503 (2019).
[31] P. Costa, H. Hansen, M. C. Ruivo, and C. A. de Sousa, Phys. Rev. D **81**, 016007 (2010).
[32] C. Sasaki and K. Redlich, Nucl. Phys. **A832**, 62 (2010).
[33] M. Motta, R. Stiele, W. M. Alberico, and A. Beraudo, Eur. Phys. J. C **80**, 770 (2020).
[34] A. Kurkela and A. Vuorinen, Phys. Rev. Lett. **117**, 042501 (2016).
[35] O. Kaczmarek, F. Karsch, F. Zantow, and P. Petreczky, Phys. Rev. D **70**, 074505 (2004); **72**, 059903(E) (2005).
[36] O. Kaczmarek and F. Zantow, Phys. Rev. D **71**, 114510 (2005).
[37] P. Wölfle, J. Schmalian, and E. Abrahams, Rep. Prog. Phys. **80**, 044501 (2017).
[38] P. Parotto, M. Bluhm, D. Mroczek, M. Nahrgang, J. Noronha-Hostler, K. Rajagopal, C. Ratti, T. Schäfer, and M. Stephanov, Phys. Rev. C **101**, 034901 (2020).
[39] J. H. Weber, A. Bazavov, and P. Petreczky, *Proc. Sci.*, Confinement2018 (2019) 166 [arXiv:1811.12902].
[40] Y. Hatta and T. Ikeda, Phys. Rev. D **67**, 014028 (2003).
[41] R. D. Pisarski and F. Wilczek, Phys. Rev. D **29**, 338 (1984).
[42] J. Berges and K. Rajagopal, Nucl. Phys. **B538**, 215 (1999).
[43] P. de Forcrand and O. Philipsen, Nucl. Phys. **B673**, 170 (2003).
[44] A. Pelissetto and E. Vicari, Phys. Rep. **368**, 549 (2002).
[45] C. Sasaki, B. Friman, and K. Redlich, Phys. Rev. D **77**, 034024 (2008).
[46] P. Costa, C. A. de Sousa, M. C. Ruivo, and Y. L. Kalinovsky, Phys. Lett. B **647**, 431 (2007).
[47] Y. Lu, Y.-L. Du, Z.-F. Cui, and H.-S. Zong, Eur. Phys. J. C **75**, 495 (2015).
[48] Y.-L. Du, Y. Lu, S.-S. Xu, Z.-F. Cui, C. Shi, and H.-S. Zong, Int. J. Mod. Phys. A **30**, 1550199 (2015).
[49] T. Dore, J. Noronha-Hostler, and E. McLaughlin, Phys. Rev. D **102**, 074017 (2020).

[50] L. Du, X. An, and U. Heinz, Phys. Rev. C **104**, 064904 (2021).
[51] C. Nonaka and M. Asakawa, Phys. Rev. C **71**, 044904 (2005).
[52] J. M. Karthein, D. Mroczek, A. R. Nava Acuna, J. Noronha-Hostler, P. Parotto, D. R. P. Price, and C. Ratti, Eur. Phys. J. Plus **136**, 621 (2021).
[53] J. Günther, R. Bellwied, S. Borsanyi, Z. Fodor, S. D. Katz, A. Pasztor, and C. Ratti, EPJ Web Conf. **137**, 07008 (2017).
[54] O. Soloveva, D. Fuseau, J. Aichelin, and E. Bratkovskaya, Phys. Rev. C **103**, 054901 (2021).
[55] O. Soloveva, P. Moreau, and E. Bratkovskaya, Phys. Rev. C **101**, 045203 (2020).
[56] J. L. Anderson and H. R. Witting, Physica **74**, 466 (1974).
[57] J. Cox, D. Wagman, and V. Medvedev, *CODATA Key Values for Thermodynamics* (Hemisphere Publishing Corp., New York, 1989).
[58] J.-M. P. Tournier and M. S. El-Genk, J. Thermophys. Heat Transfer **22**, 442 (2008).
[59] V. V. Brazhkin, Y. D. Fomin, A. G. Lyapin, V. N. Ryzhov, and K. Trachenko, Phys. Rev. E **85**, 031203 (2012).
[60] S. Ryu, J. F. Paquet, C. Shen, G. S. Denicol, B. Schenke, S. Jeon, and C. Gale, Phys. Rev. Lett. **115**, 132301 (2015).
[61] P. Chakraborty and J. Kapusta, Phys. Rev. C **83**, 014906 (2011).
[62] H. Berrehrah, E. Bratkovskaya, W. Cassing, P. Gossiaux, and J. Aichelin, Phys. Rev. C **91**, 054902 (2015).
[63] R. Marty, E. Bratkovskaya, W. Cassing, J. Aichelin, and H. Berrehrah, Phys. Rev. C **88**, 045204 (2013).
[64] N. Astrakhantsev, V. Braguta, and A. Kotov, J. High Energy Phys. 04 (2017) 101.
[65] N. Astrakhantsev, V. Braguta, and A. Kotov, Phys. Rev. D **98**, 054515 (2018).
[66] P. Kovtun, D. T. Son, and A. O. Starinets, Phys. Rev. Lett. **94**, 111601 (2005).
[67] D. T. Son and M. A. Stephanov, Phys. Rev. D **70**, 056001 (2004).
[68] F. Karsch, D. Kharzeev, and K. Tuchin, Phys. Lett. B **663**, 217 (2008).
[69] G. D. Moore and O. Saremi, J. High Energy Phys. 09 (2008) 015.
[70] H. Fujii and M. Ohtani, Phys. Rev. D **70**, 014016 (2004).
[71] P. C. Hohenberg and B. I. Halperin, Rev. Mod. Phys. **49**, 435 (1977).
[72] L. P. Kadanoff and J. Swift, Phys. Rev. **166**, 89 (1968).
[73] N. Goldenfeld, *Frontiers in Physics* Vol. 85 (Westview, Boulder, CO, 1992).
[74] A. Onuki, Phys. Rev. E **55**, 403 (1997).
[75] A. Monnai, S. Mukherjee, and Y. Yin, Phys. Rev. C **95**, 034902 (2017).
[76] J. A. Fotakis, M. Greif, C. Greiner, G. S. Denicol, and H. Niemi, Phys. Rev. D **101**, 076007 (2020).
[77] R. Rougemont, R. Critelli, J. Noronha-Hostler, J. Noronha, and C. Ratti, Phys. Rev. D **96**, 014032 (2017).
[78] H. Berrehrah, E. Bratkovskaya, W. Cassing, P. Gossiaux, J. Aichelin, and M. Bleicher, Phys. Rev. C **89**, 054901 (2014).